AD-A183 389 THEORY OF CROSS FIELD DEVICES AND A COMPARATIVE STUDY OF OTHER RADIATION SOURCES(U) NAVAL RESEARCH LAB WASHINGTON DC Y Y LAU 21 JUL 87 NRL-MR-6029 1/1

UNCLASSIFIED F/G 9/1 NL

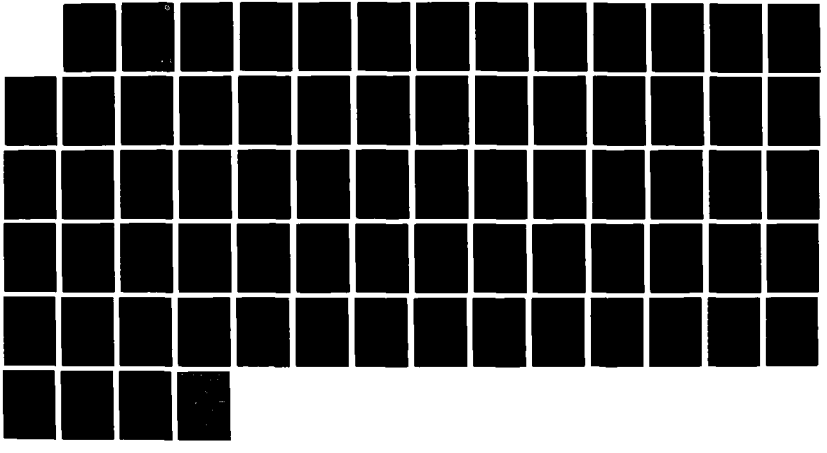

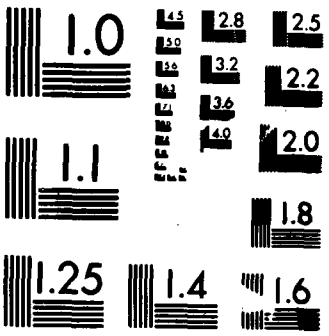

MICROCOPY RESOLUTION TEST CHART
NATIONAL BUREAU OF STANDARDS-1963-A

Naval Research Laboratory
Washington, DC 20375-5000

NRL Memorandum Report 6029

Theory of Cross Field Devices and a Comparative Study of Other Radiation Sources

Y.Y. LAU

Plasma Theory Branch
Plasma Physics Division

July 21, 1987

Supported by the Office of Naval Research

SECURITY CLASSIFICATION OF THIS PAGE A182288

REPORT DOCUMENTATION PAGE

1a. REPORT SECURITY CLASSIFICATION UNCLASSIFIED	1b RESTRICTIVE MARKINGS
2a. SECURITY CLASSIFICATION AUTHORITY	3 DISTRIBUTION / AVAILABILITY OF REPORT Approved for public release; distribution unlimited.
2b. DECLASSIFICATION / DOWNGRADING SCHEDULE	
4. PERFORMING ORGANIZATION REPORT NUMBER(S) NRL Memorandum Report 6029	5 MONITORING ORGANIZATION REPORT NUMBER(S)
6a. NAME OF PERFORMING ORGANIZATION Naval Research Laboratory 6b OFFICE SYMBOL (If applicable) Code 4790	7a. NAME OF MONITORING ORGANIZATION
6c. ADDRESS (City, State, and ZIP Code) Washington, DC 20375-5000	7b. ADDRESS (City, State, and ZIP Code)
8a. NAME OF FUNDING / SPONSORING ORGANIZATION Office of Naval Research 8b. OFFICE SYMBOL (If applicable)	9 PROCUREMENT INSTRUMENT IDENTIFICATION NUMBER
8c. ADDRESS (City, State, and ZIP Code) Arlington, VA 22217	10 SOURCE OF FUNDING NUMBERS PROGRAM ELEMENT NO: 66153N; PROJECT NO: RR011-09-41; TASK NO; WORK UNIT ACCESSION NO

11 TITLE (Include Security Classification)

Theory of Cross Field Devices and a Comparative Study of Other Radiation Sources

12 PERSONAL AUTHOR(S)
Lau, Y.Y.

13a TYPE OF REPORT	13b TIME COVERED	14 DATE OF REPORT (Year, Month, Day)	15 PAGE COUNT
Interim	FROM _____ TO _____	1987 July 21	72

16 SUPPLEMENTARY NOTATION

Supported by the Office of Naval Research

17 COSATI CODES			18 SUBJECT TERMS (Continue on reverse if necessary and identify by block number)
FIELD	GROUP	SUB-GROUP	Microwave sources; Cross field devices; Electron beam stability

19 ABSTRACT (Continue on reverse if necessary and identify by block number)

This paper gives an elementary exposition of the theory of cross field microwave devices. It provides a re-examination of the interaction mechanism in the light of the more modern radiation sources such as orbitron, gyrotron, peniotron and gyromagnetron. The treatment emphasizes simplicity and accessibility to workers not familiar with the field. The operating conditions of magnetrons will be described first, together with a qualitative description of the physical processes by which the energy of the electrons is transferred to the rf. These processes involve an interplay of the streaming motion and transverse migration of the electrons in DC electric and magnetic fields, and phase focusing provided by the rf fields of the corrugated walls. The more modern devices mentioned above are based on certain combinations of these processes, depending on the presence, or absence, of the DC electric field, of the DC magnetic field, and of the wall corrugation. The essential features of this interaction mechanism can be quantified by the use of a sheet beam model and the various radiation sources are then characterized by a single dimensionless parameter [illegible], which

(Continued)

20 DISTRIBUTION / AVAILABILITY OF ABSTRACT	21 ABSTRACT SECURITY CLASSIFICATION
☒ UNCLASSIFIED/UNLIMITED ☐ SAME AS RPT ☐ DTIC USERS	UNCLASSIFIED
22a NAME OF RESPONSIBLE INDIVIDUAL Y.Y. Lau	22b TELEPHONE (Include Area Code) 202-767-2765
	22c OFFICE SYMBOL Code 4790

DD FORM 1473, 84 MAR 83 APR edition may be used until exhausted
All other editions are obsolete

SECURITY CLASSIFICATION OF THIS PAGE

ABSTRACT (Continued)

proportional to the equilibrium electric field experienced by the sheet beam. The wall corrugation enters only in the admittance in the theory of beam-wave interaction. A small signal theory is developed from first principle for general values of h. The decisive dependence of the stability on the equilibrium type (h) is described in detail. While the validity of the simple theory has been ascertained by various vigorous tests, several important features remain to be tested in laboratory experiments. These, together with other outstanding issues, will be addressed.

CONTENTS

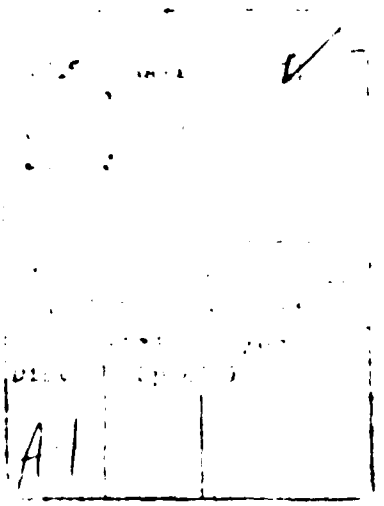

THEORY OF CROSS FIELD DEVICES AND A COMPARATIVE STUDY OF OTHER RADIATION SOURCES*

I. Introduction

Magnetron is a widely used radiation source [e.g., radar, microwave oven, etc.,]. It was developed very early but is perhaps the most complicated one to analyze theoretically[1-3]. Design studies have largely relied on empirical experiences and on the two formulas, the Hull condition and the Buneman-Hartree condition, which were derived almost half a century ago. Modern advances in electronic computing still have not provided sufficiently accurate models to confidently predict or explain the multiple facets usually observed in experiments. Such a state of imperfect understanding of the magnetrons remains in spite of the strong efforts of the many leaders of the field. Resurgence of interest in cross field devices is, in part, triggered by the more recent developments of high power diodes[4] and relativistic magnetrons[5,6].

Much of the difficulty in a theoretical study of magnetrons lies with their complex geometries. Controversy already emerged at the very first step: What should be taken as the basic motion of the electrons in a smooth bore magnetron, in the absence of rf fields? Should one take the highly idealized model of laminar flow or should one really need to use the more complicated "multi-stream" model, in which the electrons follow cycloidal orbits which commence and finish on the cathode surface? To this date, a definite answer still has not emerged, but general opinion seems to be more in favor of the laminar flow model, especially prior to full oscillation. Note that the underlying words above already indicate considerable simplification. In fact, in virtually all existing analytical

*This manuscript is prepared for *Generation of High Power Microwave and Millimeter Waves*, Eds. V. L. Granatstein and I. Alexeff (Artech House, Inc., Norwood, MA, 1987).

Manuscript approved May 4, 1987.

theories, the presence of corrugated structure is assumed to have no effect on the unperturbed motion of the electrons[7]. The wall corrugation enters only in the rf modes which are supported [Fig. 1a]. It is possible that such an assumption, made for convenience of analysis, has already eliminated a significant amount of interesting physics. [One needs not go very far to see this. For example, it is the periodicity introduced in the streaming motion of the electrons in the equilibrium state (by a magnetic wiggler) which is responsible for free electron laser action as is explained elsewhere in this volume.]

Another feature which contributes to the complexity of magnetrons is the fact that the electron-emitting cathode is part of the interaction circuit. This differs from many other microwave devices such as gyrotron[8], klystron[3], free electron laser[9], gyromagnetron[10], peniotron[11], etc., where the interaction region is separated from that of beam generation. The control of gun noises and "beam quality" becomes problematical. This, of course, is just the reason why the beam cannot be well-characterized as described in the preceding paragraphs. This problem of equilibrium-modelling appears to be an intrinsic difficulty for theorists, in those microwave sources where the rf draws directly from the electrostatic energy of the system. [Another case in point is the more recent invention of orbitron[12], where the unperturbed orbits cannot be controlled, thereby leading to a variety of interpretation and interaction theories. See below for more detail.] Actually, this may well be an advantage as far as the utility of these tubes is concerned. Such a tube should be rugged when operational, since the performance is not critically dependent on whether the beam has a superb beam quality. This insensitivity to the electron beam quality is in marked contrast to the more "delicate" radiation sources such as travelling wave tubes, free electron lasers, etc.

The magnetron circuit supports a variety of electromagnetic modes. The multiplicity of modes, together with the uncertainties in the electronic motion, greatly reduces the predictability of beam-circuit interaction. In fact, whether the beam-circuit interaction analysis, using the standard technique of impedance matching, is adequate at all in describing magnetron operation, has been questioned from the beginning. This concern was not without basis and was reviewed by J. M. Osepchuk on p. 275 of Ref. 2. It perhaps explains why the theory of magnetron lags behind those of the more modern devices mentioned earlier. But it also means that the full potential of high power radiation sources driven by direct conversion (from potential energy) remains to be realized.

With this caveat, we shall only give here an elementary exposition of some aspects of cross field devices. The laminar flow model will be adopted. The operating conditions will be given in the next section, to be followed by a qualitative description of the mechanism of energy transfer in cross-field geometries. The rf generation is a result of the interplay of wave-particle synchronism, phase focusing, conversion of both electrostatic and kinetic energy of the beam through its transverse and longitudinal motion in the rf fields supported by the corrugated walls. Some (but not all) of these features are shared by other more contemporary microwave sources such as orbitron, gyrotron, peniotron and gyro-magnetron and will be discussed in Sec. III. In fact, the comparison among these various devices form an integral part of this Chapter. This can be achieved by the use of highly idealized models which will be described in Sec. IV and V. Despite its scope, the exposition is self-contained, and a minimal amount of mathematics will be required. Detailed justification and extension of the theory will be referred to when the occasion arises. Some of the topics discussed are still under active investigation.

II. Brillouin Flows, Hull Cut-off Condition, and Buneman-Hartree Oscillation Condition

The laminar flow model which has been studied extensively in cross field devices is the Brillouin flow. It is basically an ExB drift, ignoring the cycloidal motion of the electrons [Fig. 1]. It is the mean flow field of the electron cloud with which the rf interacts over a long time scale. Although the Brillouin flow is difficult to achieve experimentally, recent particle simulation of magnetrons show that the space charge distribution and the electronic motion contain a large component of the Brillouin flow, especially during the start-up stage. In the absence of curvature effects, consideration of the planar Brillouin flow immediately leads to the Hull cut-off condition and the Buneman-Hartree condition. These conditions determine the range of voltage (at a given magnetic field) in which a magnetron operates. When curvature and relativistic effects are included, the derivation would be more involved, but the main features of these conditions remain unchanged.

One should keep in mind the assumptions used in the derivation of the Brillouin flow: (a) The flow is laminar, and is parallel to the sole.
(b) There is no variation in the direction of the flow. Thus, spatial inhomogeneity associated with the corrugated structure is ignored.
(c) All electrons are emitted from the cathode with zero velocity and zero energy. In the derivation of the cut-off condition and the oscillation condition, the rf fields, when present, are assumed to have infinitesimally small amplitude, and thus all fields are essentially static. (The last two assumptions are also used when these conditions are derived from single particle motion as in the case of a cylindrical model.) The generalization to cylindrical models with relativistic effects will be indicated.

For simplicity, we shall first consider the planar, nonrelativistic model. The governing equations for the system depicted in Fig. 1b read

$$\vec{v} = \hat{x}\, v(y) \tag{1}$$

$$-|e|V + \frac{1}{2} m_o v^2 = 0 \tag{2}$$

$$v(y) = \frac{1}{B_o} \frac{\partial V}{\partial y} = -E_o/B_o. \tag{3}$$

Equation (1) follows from assumptions (a), (b), and (2) from assumption (c) of the previous paragraph. Equation (3) accounts for the force balance in the flow field. Here $v(y)$ is the flow speed and $V=V(y)$ is the voltage distribution with $V(0)=0$ at the cathode, e is the electronic charge, E_o is the electric field consistent with the space charges and B_o is the external constant magnetic field. The diamagnetic field is ignored.

Upon differentiating Eq. (2) with respect to y and eliminating $\partial V/\partial y$ according to (3), we obtain a solution for $v(y)$:

$$v(y) = \omega_c y \tag{4}$$

where $\omega_c = |e|B_o/m_o$ is the cyclotron frequency. In obtaining (4), we have used the boundary condition $v(0)=0$. The voltage distribution reads

$$V(y) = \frac{1}{2} \frac{m_o v^2}{|e|} = \frac{1}{2} \frac{m_o}{|e|} \omega_c^2 y^2, \tag{5}$$

and the electric field is

$$E_o(y) = -\frac{\partial V}{\partial y} = \frac{-m_o}{|e|} \omega_c^2 y. \tag{6}$$

The charge density is

$$\rho_o = \varepsilon_o \frac{\partial E_o}{\partial y} = \frac{m_o}{e} \omega_c^2 \varepsilon_o,$$

which may be written as

$$\omega_p^2 = \omega_c^2,$$

where $\omega_p = (\rho_o e/m_o \varepsilon_o)^{1/2}$ is the the plasma frequency. Note that the laminar flow condition demands the condition $\omega_p = \omega_c$ be satisfied.

Given separation D, operating voltage V and magnetic field B_o, the thickness H of the space charge layer [Fig. 1b] may be calculated. Note first that the electric field equals to $-m_o\omega_c^2 H/|e|$ between the region y=H and y=D [cf. Eq. (5)]. Then the total voltage drop becomes

$$V = V(H) + \frac{m_o\omega_c^2 H}{|e|}(D - H) = \omega_c B_o H(D - \frac{H}{2}). \tag{7}$$

Solving for H, we obtain

$$H = D\left[1 - (1 - V/V_c)^{1/2}\right], \tag{8}$$

where

$$V_c = \frac{1}{2}\frac{|e|}{m_o} B_o^2 D^2 \tag{9}$$

is the Hull cut-off voltage.

Thus, the Brillouin flow is characterized by a velocity field of constant shear [cf. Eq. (4)], and by a constant charge density extending from the cathode to a distance H, which is given by (8) in terms of the voltage V, magnetic field B_o and anode-cathode separation D. The electron density satisfies $\omega_p = \omega_c$.

The Hull cut-off voltage V_c has the following interpretation. It is the maximum voltage, at a given magnetic field, allowed for magnetic insulation, i.e., for prohibiting the electrons from reaching the anode. This can be seen by setting H = D in Eq. (7). The parabolic dependence of V_c on B_o [cf. Eq. (9)] is sketched in Fig. 2. For parameters below t e Hull parabola, the magnetron is insulated. The same condition (9) is

obtained from single particle orbit considerations. An electron emitted from rest at the cathode will not be able to reach the anode if $V<V_c$, if the fields are time independent and azimuthally symmetric.

An alternate form for Eq. (8) is

$$H = D\left\{1 - \left[1 - (B_H/B_o)^2\right]^{1/2}\right\},$$

where

$$B_H = \left(\frac{2m_o V}{|e|D^2}\right)^{1/2} \tag{10}$$

is known as the Hull cut-off magnetic field. It is the minimum magnetic field required for magnetic insulation at a given voltage. When the operating voltage V is small compared with V_c, we may approximate (8) as

$$H \simeq \frac{1}{2} D\left(\frac{V}{V_c}\right) = \frac{D}{2}\left(\frac{B_H}{B_o}\right)^2,$$

which shows that the space charge layer thickness increases linearly with the voltage, but decreases as $1/B_o^2$ as B_o increases. If the operating voltage is only 1/2 of the Hull cut-off voltage, the space charge layer occupies about 1/4 of the width of the gap. It is easily shown from Eq. (8) that as $V \to V_c$, magnetic insulation is rapidly diminished.

For effective transfer of energy from the electrons to the rf, there must be synchronism between the rf wave and at least some of the electrons in the sheath. Since the ExB drift of the electrons within the sheath has a maximum speed, for rf with phase velocity v_{ph} to be synchronized with the electron at a fixed magnetic field, the voltage cannot be too low. For then the space charge layer thickness H would be small, and even the maximum electron speed $\omega_c H$ would be below v_{ph} [cf. Eqs. (4), (8)]. This minimum voltage, above which a magnetron may oscillate, is called the Buneman-Hartree threshold voltage and is determined in the present case simply by

$$v(H) = v_{ph}. \tag{11}$$

Upon using (8) and (4) in (11), the threshold voltage then becomes

$$V_{BH} = B_o D v_{ph} - \frac{m_o}{2|e|} v_{ph}^2, \tag{12}$$

which depends on the phase velocity of the mode under consideration. This threshold voltage is also shown in Fig. 2. It can easily be shown that, regardless of the phase velocity, the straight line representing the threshold voltage in Fig. 2 is always tangent to the Hull parabola.

When both relativistic and cylindrical effects are included, the Hull cut-off magnetic field and the threshold voltage are modified. If we use D_* to represent the equivalent gap width $(b^2-a^2)/2a$, [cf. Fig. 1a], the Hull cut-off magnetic field becomes

$$B_H = \left(\frac{m_o c}{|e| D_*}\right)\left[\frac{2|e|V}{m_o c^2} + \left(\frac{|e|V}{m_o c^2}\right)^2\right]^{1/2}, \tag{10a}$$

and the threshold voltage (12) is modified to read

$$V_{BH} = B_o D_* v_{ph} - \frac{m_o c^2}{|e|}\left\{1 - \left[1 - \left(\frac{v_{ph}}{c}\right)^2\right]^{1/2}\right\}. \tag{12a}$$

This relativistically correct threshold voltage was obtained by Walker[13] using a Hamiltonian description of orbits. When this threshold voltage is maximized with respect to the phase speed, the cut-off voltage [Eq. (10a)] is obtained. Again, the threshold voltage curve is tangent to the cut-off voltage curve as in Fig. 2. Magnetron oscillation takes place when V and B_o lie between these curves, but usually closer to the Buneman-Hartree threshold voltage[6]. Note that (10) and (12) are recovered from (10a) and (12a) in the nonrelativistic limit $c \to \infty$. There are recent modifications of these voltages, including the effect of diamagnetic current[14] and axial

current[15]. All of these derivations made three key assumptions: (a) the external field is azimuthally symmetric, (b) the amplitude of rf is so low that the energetics of orbital motion is not affected, and (3) the fields are time independent. In practice, none of these assumptions are valid. We refer to the Chapter by Benford[16] for a detailed discussion of the experiments and these conditions.

The validity of the old concepts outlined above has been tested in computer simulations. A. Palevsky[5] recently developed a two-dimensional, time-dependent, fully electromagnetic and fully relativistic particle simulation code to model pulsed relativistic magnetrons[17]. Some of the simulation results are shown in Figs. 3 and 4. Figure 3 shows the contour levels of charge densities at an early time, before oscillation starts. The arrows label the theoretical Brillouin layer. The corresponding velocity profile (not shown) follows the Brillouin flow to within a few percent. The contour plot at a much later time (when oscillation is fully developed) is shown in Fig. 4. The spoke formation is evident. Note that the spatial extent of the sheath is approximately given by the Brillouin layer even at this late stage when the beam-circuit interaction is highly nonlinear. The velocity profile corresponding to Fig. 4 contains considerable spread about the theoretical Brillouin flow, and confirms the considerable back-bombardment of electrons at the cathode[18]. These simulation results do show that the electron flow is a mixture of Brillouin flow and a somewhat weaker multi-stream component. They also corroborated the suggestion, made by Buneman[19] a long time ago, that the instabilities associated with such shear flows may play a key role in the start-up of magnetron oscillation. We shall return to the stability of the laminar flow later.

III. Gain Mechanism in Cross Field Devices and Comparison With Other Radiation Sources

In this section, we describe in a qualitative manner the transfer of electron energy (kinetic and potential) to the rf. We shall bring out certain features which are unique to the magnetron configuration. We shall also contrast several other microwave sources which share some, but not all, of these features. A simple theory using a beam model which is often adopted for all of these radiation sources will be given in the next section.

If the externally imposed voltage and axial magnetic fields are sufficiently strong, the average motion of the electrons is approximately the ExB drift. The curvature effect of the magnetrons is secondary in importance, and one may consider a planar model as shown in Fig. 5. Let us consider the action on electron A due to the combined DC fields E_o, B_o, and an rf electron field E_1. The rf electric field is assumed to have a phase velocity approximately equal to the unperturbed drift velocity v_o of the electron, and to have a phase shift of π from one cavity to the next, as shown in Fig. 5. The rf electric field E_1 affects the motion of electron A in four ways : (a) It retards the drift motion of the electron because E_1 and v_o are in the same direction. (A carries a negative charge). (b) The $E_1 \times B_o$ drift brings test electron A upward, to a location closer to the wall corrugation (anode), where the rf field is stronger. (c) As a result, the drift motion is retarded further, and by conservation of energy, this energy is converted to rf. (d) More importantly, as electron A drifts toward the anode, it experiences a loss of potential energy associated with the DC electric field. Again, conservation of energy requires that the potential energy be converted to the rf. These processes continue until A hits the anode.

Consider now the action of the rf electric field on test electron B [Fig. 5]. Test electron B is accelerated by the field. But this acceleration is weakened gradually since the $E_1 \times B_o$ drift brings electron B downward, toward the cathode where the rf electric field is weaker. Thus, while electron B gains energy from the rf, on the whole, the amount of energy it gains is less than the amount of energy electron A would lose to the waves, and the rf signal grows. Note that this rf growth is at the expense of both the kinetic and potential energy of the electron, the potential energy giving the dominant contribution.

The configuration shown in Fig. 5 also demonstrates the interesting property of phase focusing in magnetrons. Suppose now the phase speed v_{ph} of the rf is slightly less than the drift speed v_o of the electrons. At a later time, electron A will advance ahead of the wave, reaching a position near P relative to the wave. Near P, E_1 opposes E_o. Therefore, the electron drift velocity $(E_o+E_1)\times B_o$ is lowered, thereby reducing the difference between v_{ph} and the drift velocity. This effectively brings the electron from position P back to the original position A. For electron B, since $v_o > v_{ph}$, at a later time, it reaches position near Q with respect to the wave. Near Q, E_1 is in the same direction of E_o, therefore, the combined drift velocity $(E_1+E_o) \times B_o$ is increased, enlarging the difference between the drift velocity and the phase speed of the wave. In other words, electrons like B, which gain energy from the rf, are quickly put out of synchronism, whereas electrons like A, which give energy to the rf, will continue to do so until they reach the anode.

The same argument applies when $v_o < v_{ph}$. For example, if $v_o < v_{ph}$, electron A will lag behind the wave, moving to a position near Q with respect to the rf. At Q, the drift speed $(E_1+E_o)\times B_o$ increases since E_1

reinforces E_0 there. This effectively brings A closer to synchronism with the wave than was originally.

From the description of the last two paragraphs, one sees that there is a built-in phase focusing for the "favorable" electrons, (like A which gives its energy to the rf) and a phase defocussing of the "unfavorable" electrons, (like B which gains energy from the rf). It is this built-in focusing property which is largely responsible for the high efficiency of magnetrons. It is the reason why charge spokes are formed [cf. Fig. 4] and is perhaps a physical basis for the construction of nonlinear soliton solutions[20] which are shape-preserving.

The rather fascinating interplay between DC and AC electric fields, drift motion and the presence of corrugated structure in a cross field configuration can be contrasted with other microwave sources which share some of these features. We have in mind the peniotron, orbitron, gyrotron and gyromagnetron. All of these devices are currently under active study. They were invented more than twenty years after the magnetrons were put in service. In a sense, they are much "simpler" devices.

A model of peniotron[11] is shown in Fig. 6a. It consists of an annular electron layer rotating inside a ridged waveguide. This beam is guided only by an external magnetic field. This system differs from a magnetron in that the rf energy derives from the kinetic energy of the electron beam, the potential energy is entirely absent. (No DC electric field is present in the interaction circuit.) It is similar to the magnetron in one important aspect, however. The spatial inhomogeneity of the rf fields produced by the ridged waveguides may cause the guiding center of an electron to drift sideways, and, as a result, to turn virtually all of its kinetic energy into radiation, implying an extremely high efficiency.

To see the action of the rf field inhomogeneity on the energy transfer, consider two electrons A and B in Figs. 6b and 6c. Assume that the electrons are "nonrelativistic", (~10 KeV, as typical in peniotron) and that its cyclotron frequency is 1/2 of the rf frequency (i.e., operation at second cyclotron harmonics). Electron A is in an accelerating phase, its rotational energy increases and as a result, its radius enlarges. As its radius enlarges, it moves half a cyclotron period later to a position where the rf field is stronger, but at which time the rf field decelerates electron A. Thus electron A gives more energy to the rf during the second half of the cyclotron period than it gains during the first half. On the whole, its energy decreases and its guiding center shifts to the left (Fig. 2b). The electron energy is transferred to the rf. Electron B (Fig. 6c) is initially decelerated by the rf field and, as a result, its radius decreases. Half a cyclotron period later, electron B experiences a weaker accelerating electric field. Thus, because of the spatial inhomogeneity of the rf electric field created by the ridges, electron B loses energy to the rf during a cyclotron period and its guiding center drifts to the right [Fig. 2c]. Note that both electrons A and B yield their kinetic energy to the rf. Computer simulation shows that the decelerated electrons can virtually be stopped, leading to a theoretical efficiency close to 100 percent[22,11]. (Experimental results may be more difficult to intepret, however[21].)

The above description indicates that the mechanism of energy transfer in peniotron need not involve beam bunching along the unperturbed orbit of an electron beam. As in a magnetron, it is the transverse migration of electrons into regions of stronger rf field created by the ridges which leads to the high efficiency. For this and other reasons, the modes of operation of peniotron and cross field devices are sometimes known as the

transverse modes. A more precise definition will be given in the next section. We should also point out that the above description is not the only possible mechanism responsible for the radiation generated in a peniotron[21]. We shall say more about this at the end of this section, where we treat the gyromagnetron[10,23]. The gyromagnetron is topologically identical to the peniotron, but is envisioned to operate with an entirely different mechanism.

Orbitron[12] is similar to a magnetron in that an electrostatic field is present, and that the rf derives most of its power from the electrostatic field. A model of orbitron which has been subject to some theoretical study is shown in Fig. 7. In this figure, a cylindrical layer of electrons rotates about a center wire which is positively charged with respect to the outer cylinder. The radial electrostatic field provides the centripedal acceleration and no external magnetic field is present[24]. In some sense, the orbitron may be considered as diametrically opposite to the peniotron, in that one uses only an electrostatic field for electronic motion whereas the other uses only a magnetic field. Moreover, one relies on complicated wall structures whereas in the other, a smooth wall suffices, in which case the importance of rf field inhomogeneity diminishes.

Since the role of rf field inhomogeneity is minimal in an orbitron, the only way for the beam to yield its energy (kinetic and potential) is via a bunching mechanism along the particle orbit for the model shown in Fig. 7. This is indeed found to be the case. Suppose that some charge perturbation is set up on the beam. A test electron moving ahead of this charge bunch is accelerated, it moves outward to a larger radius. This leads to a decrease of the rotational frequency since the regular frequency decreases like $1/r$ for an electrostatically focused beam [Fig. 7]. Azimuthally, this test electron moves toward the bunch and behaves as if

having a "negative inertia" ------ it falls back toward the bunch upon being pushed[12,27,28]. Similarly, a test electron which is initially behind the charge perturbation is decelerated, it moves to a smaller radius, but its angular frequency increases, effectively catching up with the bunch azimuthally. Thus there is strong tendency for beam bunching in the orbitron configuration shown in Fig. 7. In fact, we shall show in the next section that this negative mass behavior is indeed very pronounced ----- far more pronounced than that exhibited in a large orbit gyrotron at low beam energy (<10 KeV) [See Eq. (27) below].

A highly bunched beam can readily yield radiation. In so doing, the beam contracts radially in an orbitron. It falls to a region of lower potential energy. It can easily be estimated that the radiation draws energy primary from the electrostatic energy like in a magnetron. However, as the beam falls toward the center wire, its angular frequency may be considerably detuned from the mode of operation, thereby limiting the operating efficiency. Unless some form of phase-focusing is introduced, orbitrons cannot be expected to yield efficiencies comparable to magnetrons. Thus, the model shown in Fig. 7 has the peculiar property that it yields tremendous small signal gain, but the efficiency may be modest.

The electron beam in a large orbit gyrotron [Fig. 8a] requires an external axial magnetic field to provide the rotation. There is no externally imposed DC electric field in the circuit. In the simplest geometry, the wall corrugation is absent and the transfer of energy is through charge bunching along the beam orbit [Figs. 8a, 8b]. Similar to the orbitron, the bunching is enhanced by a negative mass effect. Here, the negative mass effect is relativistic in origin, but is already noticeable when the beam energy is beyond keV. If there is a charge

perturbation in the electron beam, test electron A in front of the bunch is accelerated. Its rotational frequency $\omega_o = |e|B_o/m_o\gamma_o(A)$ decreases as its relativistic mass factor $\gamma_o(A)$ is increased. Azimuthally, therefore, A falls back to the bunch as a result of this relativistic mass effect. Similarly, electron B is decelerated, $\gamma_o(B)$ decreases but its angular frequency $\omega_o(B) = |e| B_o/m_o\gamma_o(B)$ increases. Azimuthally, B speeds up and catches up with the bunch [Fig. 8b]. The negative mass instability thus developed was shown to be identical to the cyclotron maser instability which leads to radiation in gyrotrons. However, it will be shown that, at low energy beam (<10KeV), the small signal gain in a gyrotron is considerably smaller than the orbitron. On the other hand, the efficiency of gyrotron may be noticeably higher since the magnetic field can be detuned so that ω ω_o is sufficiently small to yield appreciable gain, but large enough to yield substantial efficiency[8].

Gyrotron is tuned by the axial magnetic field. The magnetic field requirement can be substantially reduced if the tube can operate efficiently at a high cyclotron harmonic. A promising way to encourage harmonic operation is to introduce corrugation at the waveguide wall [Fig. 8c]. This would allow efficient operation even at low beam energy. Such an interesting possibility was predicted theoretically[10] and verified experimentally when electron beams with energy at tens of KeV were employed[11] to operate at high cyclotron harmonics. The resemblance of the magnetron outer wall, together with the gyrotron mechanism, leads to the name gyro magnetron. We should emphasize that this interpretation of the gyro magnetron relies on the longitudinal bunching of the beam, similar to [illegible] normally, given to penotron [illegible] therefore, [illegible]

gyro-harmonictron, or harmonic gyrotron, have later been used for gyromagnetron. But none of the latter names would suggest the gyrotron mechanism enhanced by a magnetron waveguide. [Ref. 10 contains a lengthy description of the historical development up to 1982.]

Comparing Figs. 8c and 6a, one immediately sees that the topologies of the gyro-magnetron and of the peniotron are identical! Both employ annular beams, ridged waveguides, and only an external magnetic field is used to provide the electron rotation. Even the beam energy and frequency range in existing experiments are similar. The immediate question is: How important is the transverse peniotron mode in the operation of gyromagnetron, and vice versa. Phrased more bluntly, the question becomes: Is the peniotron really a cyclotron maser in disguise? Or does a gyromagnetron really operate according to what is envisioned to happen in a peniotron? These are interesting questions which have generated considerable controversy, and a resolution is not immediate[29]. Thus, given the magnetic field, beam and circuit parameters, one cannot even predict with complete confidence in which mode the tube should operate[21,29]!

If the simple peniotron/gyro-magnetron configuration can cause uncertainties in our understanding of their operation at this late stage, just due to the corrugation of the waveguide circuit, it would hardly be surprising that the situation in magnetron would be much worse since there is not even a consensus in the choice of a suitable equilibrium model, not to mention a host of other complex features[6] and the highly nonlinear behavior. It then seems desirable to restrict here to a tractable theory which can cover the effects of corrugated structure, curvature and relativistic mass effects, for an electron flow under a general combination of DC electric field and magnetic field, with the effects of the AC and DC self field included. Such a theory will be presented in the following

sections by the use of a simple model (Fig.9). There, we shall isolate the circuit effects and the intrinsic beam stability, and examine their coupling.

IV. Stability of Laminar Flows

We shall now give a simple exposition of the various types of instabilities encountered in cross field devices. These instabilities have been invoked to explain the intense noise observed and the initial stages of spoke formation[2]. For simplicity of mathematics and for ready comparison with other radiation sources, only the electron sheet model shown in Fig. 9 will be covered in some detail. Though highly simplified, this sheet model retains the essential features of the physical mechanism described in the previous sections. It also demonstrates the profound effects of the equilibrium type on the stability of an electron beam. These effects were noticed only in recent years. In fact, to what extent would they enter in the case of a thick beam remains unanswered. It is highly probable that the effects are large, since different waves may be excited across a thick shear layer and they may interact. We shall address some of these issues in the next section.

We shall begin with the "longitudinal mode". The real part of the frequency ω of the longitudinal modes satisfies

$$\omega \simeq \ell \omega_o \tag{13a}$$

where ℓ is the azimuthal mode number and ω_o is the angular frequency of rotation of the electron. When a longitudinal mode is present, an electron experiences the rf field at an almost constant phase since its Doppler frequency $\omega - \ell \omega_o \simeq 0$, and there would be a strong interaction between the electron beam and the rf. This is particularly true if ω is also close to the natural mode of the circuit. The longitudinal modes are important in gyrotron, orbitron, and in cross field devices.

The frequencies of the "transverse modes" satisfy

$$\omega - \ell \omega_o \simeq \pm \kappa \tag{13b}$$

where κ is a natural frequency of oscillation about the equilibrium when an

electron orbit is perturbed. [e.g., $\kappa = eB_o/mc$ for gyrotron, peniotron, and the planar magnetron, but $\kappa = \sqrt{2}\,\omega_o$ for the orbitron model (Fig. 7) where an electron circulates under a central force field, generated by a positively charged thin wire, with 1/r dependence]. The peniotron is thought to operate with the transverse mode[11,22,29]. The transverse mode is also an important one in cross field configurations[19].

Both transverse modes and longitudinal modes have been formulated exactly[27,28] for a cylindrical laminar flow of arbitrary density profile, including DC and AC space charge effects for a general combination of radial electric field $E_o(r)$ and axial field $B_o(r)$. When specialized to a thin sheet [Fig. 9], a simple dispersion relation has been obtained. The theory presented below will highlight the remarkable features which are confirmed by a direct numerical solution of the exact eigenvalue problem.

(A) Longitudinal Instability

The free energy which drives the longitudinal modes unstable may either be the potential energy or the kinetic energy. The potential energy may arise from the DC space charge of the electron beam, in which case the "diocotron instability" is excited[30-36], or from the externally imposed potential, as in the orbitron model. In the latter case, the negative mass instability is excited. On the other hand, it is the kinetic energy of the electrons which is converted to the rf in gyrotrons. As we have explained, it is also the negative mass instability which is responsible for the radiation generated in gyrotrons[36]. The transition of these various instabilities, and their relative importance in different regimes, will be covered in the following subsections.

(A1) Diocotron Instability ----- An instability caused by DC space charges

The diocotron instability[30-33,19] was discovered during the initial phase of magnetron research. It was also one of the first plasma instabilities ever discovered. The free energy which drives this instability resides solely with the electrostatic energy of the self field of the electron sheet. There are several (equivalent) ways to view this instability. Two of them are given below for the model shown in Fig. 10, which is a further simplification from the model in Fig. 9.

The original papers attributed the diocotron instability to a hydrodynamic instability of shear flow[30]. The velocity shear is due to the self field of the electron sheet, which is assumed to have a small, but finite thickness. In fact, it was found that the diocotron instability has the same growth rate as the Kelvin Helmholtz instability of a vortex sheet in classical hydrodynamics[37]. The evolution of the instabilities, such as the curling up of the sheet, is also similar.

Associated with the DC self field of the electron sheet is a velocity shear [Fig. 10a] in the equilibrium ExB drift. The velocity differential due to self field is

$$\Delta v = \frac{E_s}{B_o} = \frac{\rho_o \tau}{\varepsilon_o B_o} = \frac{\sigma_o}{\varepsilon_o B_o},$$

where E_s is the total change of the self electric field across the electron layer of thickness τ and constant electron density ρ_o. Note that Δv depends only on the surface charge density σ_o, but is independent of the thickness τ. It provides a good approximation for a general density profile if τ is sufficiently small. The growth rate of the Kelvin Helmholtz instability in a thin vortex sheet is[37]

$$\omega_i = \frac{1}{2} k\Delta v$$

$$= \frac{1}{2} (k\tau)\omega_p^2/\omega_c, \qquad (14)$$

where k is the wave number in the direction of flow. Expression (14) is the diocotron growth rate of a thin electron sheet in the long wavelength limit $k\tau << 1$. Note that the growth rate is proportional to the beam current.

An equally transparent way to see the physical origin of the diocotron growth is through the process depicted in Figs. 10b,c. Suppose that a sinusoidal ripple is introduced on the electron sheet [Fig. 10b]. Electrons in positions A, C experience an electrostatic force in the upward direction, due to the electrons in their immediate neighborhood. Electrons in positions B, D experience a similar force, but in the downward direction. These forces produce an FxB drift to the left for electrons at A, C but to the right for electrons at B, D. This leads to an accumulation of charges between B C and a deficiency of charges between A B [Fig. 10c]. The electric field associated with these charge perturbations, as shown in Fig. 10c, produces an ExB drift of electrons which reinforces the original ripple, and the instability grows as a result.

The diocotron effect was considered to be a major cause for the intense noise and fluctuation observed in cross field devices and high power diodes. It was also thought to contribute to a significant increase of the gain in the theories of cross field amplifiers[2,3]. There are many refinements of the diocotron instabilities, such as the effects of finite beams, of geometries, and of finite Larmor radius . They are given in the literature quoted in Refs. 30-36. Instead of going into these topics, we

shall stick to the thin layer model [Fig. 9] so as to bring out the crucial dependence of stability on the equilibrium type. For example, we shall show below that the diocotron instability may be stabilized if the curvature effects are taken into account.

(A2) General longitudinal instability without DC space charge effects [negative mass, cyclotron maser, orbitron modes, etc.].

The curvature and relativistic effects have been ignored in the above description of the diocotron instabilities. In practice, in many radiation sources the curvature effects of the electron orbits are crucial. The relativistic effect may already be important for an electron beam with energy as low as 5 KeV, as shown in the original experiments on cyclotron maser[38]. To examine all of these, we now pretend in this subsection that the electron layer is neutralized to rule out the diocotron instability. The questions become: Does it make a difference in the stability if the equilibrium rotation is supported by a radial electric field alone (like an orbitron), or by an axial magnetic field alone (like a large orbit gyrotron) or by a combination of both (like a smooth bore magnetron)? How and in what way would the relativistic effects enter? All of these questions can now be answered with the following simple study.

Consider a thin, neutralized electron layer rotating concentrically at velocity $\vec{v}_o = \hat{\theta}\, v_o(r) = \hat{\theta} r\omega_o(r)$ inside some waveguide structure [Fig. 9]. The E-layer has a small thickness τ, and uniform charge density extending from $r=r_1$ to $r=r_2$ with mean radius R. For the time being, we shall leave unspecified the relative strength of the radial electric field E_o and the vertical magnetic field B_o which are needed to provide the circular motion of the beam. Thus, v_o is governed by

$$\gamma_o \frac{v_o^2}{r} = - \frac{e}{m_o} (E_o + v_o B_o). \qquad (15)$$

It is convenient to introduce a dimensionless quantity h to characterize the strength of the electric field of the equilibrium:

$$h = \frac{-erE_o}{m_o \gamma_o^3 v_o^2}. \qquad (16)$$

Note that $\gamma_o^2 h$ is equal to the ratio of the electric force to the centrifugal force in equilibrium[39]. Using this definition and the equilibrium condition (15), one may characterize the equilibrium type according to the value of h [Fig. 11]:

(i) h=0 corresponds to the large orbit gyrotron [Fig. 8], where the equilibrium rotation is supported by an axial magnetic field alone (E_o=0).

(ii) $h=1/\gamma_o^2$ corresponds to the orbitron model [Fig. 7], in which the rotation is supported solely by a radial electric field. [B_o=0, cf. Eqs. (15), (16)].

(iii) $h>>1/\gamma_o^2$ corresponds to an <u>inverted</u> magnetron, with the cathode at the outer conductor and the anode at the inner conductor. The rotation is approximately given by the ExB drift (Centrifugal force is small).

(iv) $h<<-1/\gamma_o^2$ corresponds to a conventional magnetron, with the cathode at the inner radius and the anode at the outer radius. Again, the rotation is approximately given by the ExB drift and the centrifugal force is small compared with either the electric or Lorentz force in equilibrium.

(v) The planar limit is recovered formally as $r \to \infty$ (fixing E_o, v_o). That is, $|h| \to \infty$ corresponds to the planar limit [cf. Eqs. (15), (16)].

These various special values are labelled on the h axis in Fig. 11 and a simple dispersion relation is derived below for general values of h. Since we are examining only the longitudinal modes, the beam interacts with an rf field mainly through the azimuthal component of the electric field ($E_{1\theta}$) which the thin beam experiences. Conservation of energy gives

$$ev_o E_{1\theta} = d\varepsilon/dt \tag{17}$$

where ε is the total energy (kinetic and potential) of the electron beam. Upon using the chain rule, we express

$$d\varepsilon/dt = (d\dot{\theta}/dt)/(d\dot{\theta}/d\varepsilon) = (\ddot{\eta}/R)/(d\dot{\theta}/d\varepsilon)$$

in terms of the azimuthal displacement η of an electron from its unperturbed position. Thus, (17) becomes, upon linearization,

$$\ddot{\eta} = eRv_o E_{1\theta}\left(\frac{d\omega_o}{d\varepsilon}\right) \equiv eE_{1\theta}/M_{eff} \tag{18}$$

where the equilibrium value $\dot{\theta}=\omega_o$ is expressed as a function of the particle energy. In analogy with the force law "F=ma", we define in (18) an effective mass $M_{eff} = (Rv_o d\omega_o/d\varepsilon)^{-1}$. It is not difficult to show from (15) and (16) that

$$M_{eff} = -m_o\gamma_o\left(\frac{1 + \gamma_o^2 h^2}{\beta_o^2 + 2h}\right), \tag{19}$$

where $\beta_o = v_o/c$.

Equations (18) and (19) are very interesting. They govern the longitudinal (azimuthal) dynamics of the electron beam. The crucial properties of gyrotron, orbitron, gyromagnetron, smooth bore magnetron and

its inverted configuration, or even cyclic particle accelerators such as betatrons are contained in this effective mass. Relativistic effects, curvature effects, and the magnitude and sign of h determine this effective inertia, which in turn determines the response of an electron to an accelerating or decelerating rf electric field. For example, M_{eff} is negative for $h>-\beta_o^2/2$, is positive when $h<-\beta_o^2/2$, is infinite at $h=-\beta_o^2/2$, and has a local maximum when $h=1/\gamma_o^2$ [Fig. 12]. All of these are interesting properties and will be considered shortly. Note for the time being that the main dynamical properties associated with the equilibrium type for the longitudinal modes are already contained in (18), (19).

For a perturbation proportional $\exp[j\omega t-j\ell\theta]$, d/dt stands for $j(\omega-\ell\omega_o)$ where ℓ is the azimuthal mode number. Associated with the azimuthal displacement η is a surface charge density perturbation σ_1, given by

$$\sigma_1 = -\frac{\sigma_o}{R}\frac{\partial\eta}{\partial\theta} = \frac{i\ell\sigma_o}{R}\eta$$

$$= \frac{-i\ell\sigma_o}{R}\frac{eE_{1\theta}}{(\omega-\ell\omega_o)^2 M_{eff}}, \qquad (20)$$

in which $E_{1\theta}$ is understood to be the value evaluated at r=R. In writing the last expression, we have used (18). Equation (20) expresses the charge density perturbation in the beam in response to some imposed azimuthal electric field. Thus far, the surrounding electromagnetic structure has not entered into consideration.

To complete the analysis, we calculate what kind of electromagnetic waves would be excited if there is an RF surface charge σ_1 located at r=R. The presence of a surface charge σ_1, by Gauss law, produces a discontinuity in the radial component of the RF electric field E_{1r}. Thus

$$E_{1r}^{+} - E_{1r}^{-} = \sigma_1/\varepsilon_o, \tag{21}$$

where, and in what follows, the superscript $+(\ )$ is used to designate the position just outside (inside) of the radius under consideration. We next express $E_{1r}^{\pm}$ in terms of $E_{1\theta}^{\pm}$ by introducing the wave admittances b_+ and b_- at the outer and inner edges of the beam. Specifically, b_+ and b_- are defined by

$$b_+ = iE_{1r}^{+}/E_{1\theta}^{+}, \tag{22}$$

$$b_- = iE_{1r}^{-}/E_{1\theta}^{-}. \tag{23}$$

Since the tangential electric field ($E_{1\theta}$) is approximately continuous across the electron layer, we have $E_{1\theta}^{+} \approx E_{1\theta}^{-} = E_{1\theta}$ and hence (21) (23) give

$$\frac{\sigma_1}{\varepsilon_o} = i(b_+ + b_-)E_{1\theta}. \tag{24}$$

Whereas Eq. (20) expresses the dynamical response of the beam to an rf electric field without reference to the circuit, Eq. (24) gives the circuit response to some beam excitation (σ_1), irrespective of how σ_1 is produced dynamically. For self consistency, we obtain from (20), (24) the dispersion relationship

$$(\omega/\omega_o)^2 \approx \frac{i\omega_a^2}{(b_+ + b_-)(M_{eff}/m_o\gamma_o)} \approx \omega_p^2 \frac{i(\tau - R)}{(b_+ + b_-)} \left[\frac{\beta_o^2 + 2b}{1 + \gamma_o^2 b^2}\right], \tag{25}$$

where

$$\omega_a^2 \approx \frac{2(c^2 - R^2)v}{\gamma_o} \approx \frac{Ne^2}{2\pi\varepsilon_o m_o \gamma_o R^2}. \tag{26}$$

In (26), $N=2\pi R\sigma_0/e$ is the charge number density per unit axial length, ν is the dimensionless 'Budker parameter' measuring the beam density (current) [$\nu=Ne^2/4\pi\varepsilon_0 m_0 c^2$ in MKS units, it equals to e^2N/m_0c^2 in CGS units.]

The dispersion relationship (25) governs the longitudinal stability of a model electron sheet in orbitrons, gyrotrons, gyromagnetron, and (smooth bore[7]) magnetrons. The effects of the waveguide wall enter only in the normalized wave admittance $b_+ + b_-$ in (25) and the dynamics (equilibrium type) enters in the factor $(\beta_0^2 \cdot 2h)(1+\gamma_0^2)$, which is also the mass factor in Eq. (19). The wave admittance b_+ and b_- is a function of geometry and of frequency ω, and for the longitudinal modes we are studying, $\omega=\ell\omega_0$. The mathematical expressions of b_+ and b_- for various cases are given in Appendix B of Chernin and Lau[28]. The major points are as follows. When the waveguide walls are lossless, b_+, b_- are real. It can either be positive or negative. When it is positive (negative), the beam is said to experience a capacitive (inductive) structure[40]. For frequency ω close to cut off frequencies (ω_g) of the vacuum waveguide mode, $b_+ + b_- \propto(\omega-\omega_g)$, and the growth rate becomes large, regardless of the sign of M_{eff}. Under this condition (synchronous condition), (25) becomes a cubic polynomial of $(\omega-\ell\omega_0)$, leading to a rate of growth (gain) proportional to $I^{1/3}$, which is characteristic of gain in longitudinal interactions, as in gyrotrons[40,36,41,8]. These statement on the wall admittances may be extended to the cases where the waveguide wall become corrugated, as in a gyromagnetron[15].

For convenience of discussion of the beam dynamics, we shall assume that $b_+ + b_-$ is real and positive, (except where stated). We may then, the following simple interpretation to the terms in the electron beam:

(a) When h=0, Eq. (25) indicates that an instability exists as a result of the relativistic effect. This is the well known negative mass instability[42,40], whose growth rate is given by $\omega_i^2=\omega_p^2(\ell\tau/R)\beta_o^2/(b_++b_-)$ which vanishes in the nonrelativistic limit $\beta_o\to 0$. This instability was predicted; and it places a limit on the beam current in cyclic accelerator. It turns out to be identical to the cyclotron maser instability[36], which is responsible for the radiation generated in gyrotrons.

(b) The negative mass growth rate would be present as long as $h>\beta_o^2/2$. It is maximized with respect to h when $h=1/\gamma_o^2$, as readily demonstrated from Eq. (25). This case corresponds to the orbitron configuration [Figs. 11,12]. In other words, for a given rotational energy and a given geometry, the negative mass effect is most pronounced when the equilibrium is supported by a radial electric field alone as in an orbitron model[27,28]. By setting h=0 and $h=1/\gamma_o^2$ in (25), we obtain the comparison of the small signal growth between a large orbit gyrotron and an orbitron

$$\frac{\omega_i(\text{orbitron})}{\omega_i(\text{gyrotron})}=\frac{1}{\beta_o}. \qquad (27)$$

Since β_o equals to 0.044, 0.14, 0.37, 0.55, 0.78 when the rotational energy is 1KeV, 5KeV, 40KeV, 100KeV, and 300KeV, respectively, one sees that the small signal gain for an electron layer in an orbitron configuration can in principle be rather high in comparison with the other radiation sources, especially at low beam energy. A potential use of this enhanced charge bunching in klystrons has been suggested recently[43].

(c) The dispersion relation (25) suggests that the negative mass instability is suppressed if

$$h < \beta_0^2/2. \tag{28}$$

That is, the negative mass instability may be stabilized by a negative radial DC electric field of a suitable magnitude. In terms of an external potential V imposed between the inner conductor at r a and the outer conductor at r b [See Fig.1c below], the stability condition (28) reads

$$|eV| > \left|\frac{m_0c^2}{2}\right|\beta_0^4\gamma_0^3\ln(b/a). \tag{29}$$

Note that this stabilization mechanism is independent of the beam velocity speed, and is insensitive to the beam current or container geometry, or mode number[22]. Unfortunately, it is not practical to stabilize a high energy electron beam against the negative mass instability by this method due to γ_0^3 dependence in (29). It becomes attractive, however, if this method is applied to cyclic acceleration of high energy ions ($\sim$ 500 MeV) of intermediate atomic mass (atomic number of order twenty).

Points (a), (b), (c) are illustrated (Fig. 13) for two cases, with nonrelativistic and relativistic beam kinetic energies (1KeV and 300KeV). The growth rates shown in this figure already include the (weaker) diocotron effects and will be described more fully later.

(d) If the wall is lossy, $k_z b$ becomes complex and the resistive instabilities would result[23,24] whether the effective mass is positive or negative[24,25]. However, even this resistive instability can be stabilized if $h < \beta_0^2/2$, as is evident in the dispersion relation (25)

Physically, when $h = \beta_o^2/2$, the effective mass of a rotating electron is infinite [cf. Fig. 12]. The beam is very rigid azimuthally and is incapable of transferring its rotational energy to the resistive wall, which is the physical mechanism for the excitation of the resistive instability[46].

(e) The negative mass instability should disappear in the planar geometry limit, as expected intuitively. This is also reflected in the dispersion relation (25). In this planar limit $R \to \infty$, $\ell \to \infty$, but ℓ/R, τ, E_o remain finite. Then $h \to \infty$ by (16) and the right hand member of (25) tends to zero. What remains is then the diocotron instability which is not included in (25) since the self field has been explicitly ignored in the derivation of (25).

Viewed slightly differently, we may regard (25) as the lowest order dispersion relation when we expand the growth rate in terms of the small parameter (τ/R). The diocotron growth rate (14) is the residual instability when the curvature effect is absent[39]. This, in fact, is found to be the case in an exact formulation of the eigenmodes. This will be discussed next, and examples will be given to demonstrate the validity of the growth rate formulas (25) through a direct numerical integration of the exact eigenvalue problem.

(A3) An exact formulation and the verification of the simplified dispersion relation

The implication outlined above [illegible] based on the highly simplified [illegible] given there. [illegible] to both analytical and numerical [illegible] an exact [illegible] [illegible] [illegible][27,28]. The [illegible] supported by [illegible].

combination of radial electric field and axial magnetic field with self consistent density and velocity profiles. It is fully relativistic and fully electromagnetic; it includes both DC and AC space charge effects. For TE modes with dependence $\exp(j\omega t - j\ell\theta)$, the eigenvalue equation for $\phi = rE_{1\theta}$ is of the form[27,28]

$$\frac{d}{dr}\left(A\frac{d\phi}{dr}\right) + B\phi = 0, \tag{30}$$

where A and B are rather complicated functions of ω, ℓ and r. This eigenvalue equation governs both the longitudinal modes and the transverse modes. These modes manifest themselves as singularities of the equation. The complex eigenfrequencies $\omega=\omega(\ell)$ for both types of modes are obtained by matching the solutions of ϕ at the beam edges to those of the vacuum solution exterior to the beam [or $\phi=0$ at the conducting boundary with which the electron sheath happens to be in contact.]

The eigenvalue equation (30) has been solved both analytically and numerically for a thin beam. In the analytic procedure[47], we expand all quantities in powers of (τ/R). To two orders in (τ/R), the growth rate is given by[27,28]

$$\omega_i^2 = \left(\frac{1}{b_+ + b_-}\right)\omega_p^2\left(\frac{\ell\tau}{R}\right)\frac{(\beta_o^2+2h)}{(1+\gamma_o^2h^2)} + \frac{\ell^2\tau^2}{R^2}\Lambda\omega_o^2, \tag{31}$$

where

$$\Lambda = \frac{1}{4}\frac{1}{\gamma_o^6(1+h)^2(1+\gamma_o^2h^2)}$$

$$\times\left\{\left[\frac{\omega_p^2}{\omega_o^2}\right]^2\left[\beta_o^2+2h+(1+h)^2\right]+2\left(\frac{\omega_p^2}{\omega_o^2}\right)\gamma_o^4(\beta_o^2+2h)^2-\gamma_o^6(1+\gamma_o^2h^2)(\beta_o^2+h)^2\right\}$$

$$\left[1-\frac{(1+h)\omega_p^2}{\gamma_o^2(1+\gamma_o^2h^2)}\left(\frac{b_+-b_-}{b_++b_-}\right)\right]^2. \tag{32}$$

All quantities in this expression has been defined in the previous section. Note that the first term of (31) is the same as the rhs of (25) except for the generalization[39] of h in (31). In the planar limit $R\to\infty$, $\ell\to\infty$, $\ell/R\to k$ = finite, then $h\to\infty$, and the first term of (31) disappears. Using the last term of (31), and noting that only the term involving ω_p^4/ω_o^4 remains in this planar limit, we obtain

$$\omega_i^2 = (k^2\tau^2/4\gamma_o^4)\omega_p^4/\omega_c^2.$$

This equation is just the relativistic version of the diocotron instability for a sheet beam [cf. Eq. (14), also Ref. (33)]. Thus, the diocotron instability is in fact recovered, and the negative mass instability removed, in the planar limit. In other words, Eq. (31) includes both the DC and AC space charge effect.

For a thin beam, the second term in (31) is using negligible compared with the preceding term. Thus, stabilization of the negative mass instability by the use of the criterion (28) would also imply stabilization of the diocotron instability for a thin beam. Figure 13 shows the growth rates according to the dispersion relation (31) in two examples. The interesting features are noted there: (a) maximum small signal growth for orbitron configuration ($h=1/\gamma_o^2$); (b) stabilization of negative mass and diocotron instability when $h\leq-\beta_o^2/2$; (c) persistence of small signal growth at low beam energy for gyrotron (h=0). This growth is due more to the diocotron effect than to the negative mass effect. [See Ref. 36 for more detail.]

The validity of the analytic theory has been confirmed[28] by comparing the growth rates with those obtained from direct numerical integration of the governing differential Eq. (30). Shown in Figs. 14,15 are some examples of this comparison. The solid curves represent the eigenvalues

according to numerical integration of (30) and the dashed curves to (31). Note that the stability condition and the peak growth rate predicted for orbitrons, according to (25), are confirmed in Fig. 14. The agreement in the dependence on beam current (Fig. 15) is remarkable. Other checks on geometry, on mode number, on γ_o, on τ/R, etc., have been performed[28]. They all confirm the validity of the analytic dispersion relation (31).

B Transverse Instability

The longitudinal modes described in the previous section rely heavily on the spatial inhomogeneity of the unperturbed motion [e.g., velocity shear due to space charge in the diocotron instability, and differential rotation in the negative mass instability as reflected in the effective mass factor $d\omega_o/d\varepsilon=(d\omega_o/dr)/(d\varepsilon/dr)$]. The spatial inhomogeneity of the rf field plays a secondary role. Near synchronism, the growth rates of these modes are proportional to $I^{1/3}$. In contrast, the gain mechanism in both cross field configuration and peniotron, the spatial inhomogeneity of the rf field plays a crucial role. This situation arises since the transverse drift of the "favorable" electrons, acted on by the rf fields, progressively populate a region with stronger rf fields, whereas the "unfavorable" electrons drift to a region of weaker rf field. The small signal gain for the transverse mode is proportional to $I^{1/2}$.

For the present sheet beam model [Fig. 9], the transverse modes are characterized by

$$(\omega-\ell\omega_o) \simeq \pm (1 + \gamma_o^2 h^2)^{1/2}\omega_o. \qquad (33)$$

One can readily show that the frequency $(1+\gamma_o^2h^2)^{1/2}\omega_o$ represents the radial oscillation of an electron about its guiding center in a frame co-moving with the wave, under the combined action of E_o and B_o. For example, in the

nonrelativistic limit of orbitron configuration ($h=1/\gamma_o^2 \to 1$), this frequency becomes $\sqrt{2}\ \omega_o$, which is the frequency of radial oscillation, about the guiding center, of a particle under a central force field whose strength behaves as 1/r [Fig. 7]. In another limit $h=0$, $\omega_o \to \omega_c$ (33) becomes $\omega - \ell\omega_c \simeq \pm\omega_c$ which represents gyro-resonance[2,3,11,19,28-33,40,41].

As mentioned earlier, the transverse modes are also governed by the same differential equation (30). Using the same analytical procedure which leads to the dispersion relation (31), we obtain the dispersion relation for the transverse modes for a thin electron layer[28]:

$$(\omega-\ell\omega_o)^2-(1+\gamma_o^2h^2)\omega_o^2 = \frac{-\ell\tau}{R(b_+ + b_-)}\left(\ell^2\omega_p^2\right)\left(1-\frac{\beta_o^2\omega}{\ell\omega_o}\right)\left[\left(\frac{b_+}{\ell}-q\right)\left(\frac{b_-}{\ell}+q\right)\right]. \quad (34)$$

Here

$$q \equiv -\omega_o(1+h)/[\ (\ell - \beta_o^2\omega/\omega_o)\ (\omega - \ell\omega_o)]. \quad (35)$$

This is the lowest order dispersion relationship in the expansion parameter τ/R. It is valid for general combination of E_o and B_o, and, since in this case, DC space charge is not critical, it gives the correct result in the limit of planar geometry.

This dispersion relation is rather complicated. The wave admittance b_+ and b_- reflects the corrugation of the walls and the rf field inhomogeneities such corrugation produces[10,22,32,41]. Without going into the details, we may make the following remarks.

(a) In the absence of wall loss, small signal growth can occur only when the transverse mode is synchronous with the circuit mode, for which $b_+ + b_- \simeq 0$. The growth rate under such a synchronous condition is proportional to $I^{1/2}$. This small signal growth is typically weaker than that associated with the longitudinal modes.

(b) Since synchronism is always required for small signal growth the relative importance among the centrifugal force, Lorentz force, or electrostatic force in supporting the equilibrium seems to be less important. That is, the transverse mode is perhaps less sensitive to the equilibrium type. But the resistive instabilities are equally serious for both transverse modes and longitudinal modes.

(c) Conventional theories of transverse modes also express the gains in terms of the rf electric fields (and their gradients) at the beam location[34,41]. Equation (33) is a generalization, including a possible radial electric field in a curved geometry.

(d) Numerical simulations indicated that the transverse modes, in principle, can be a very efficient mode to operate at as in peniotrons[22,29]. The small signal theory only gives the initial stage of the development. The effects of the spatial inhomogeneities of the rf field are incorporated in b_+ and b_-, which are complicated expressions themselves when ridges are present in the waveguide walls. Much work remains in the study of the transverse modes, especially their possible coupling with the longitudinal modes when the sheath thickness is no longer small.

V. Remarks

A rudimentary theory is given for a class of radiation sources in which the basic electron flow may be regarded as laminar. Emphases have been placed on the dynamical dependence of the equilibrium type and on the role of circuit structure. In general, the spatial inhomogeneities of the rf fields are important when the transverse migration of the electrons is essential, as in cross-field devices and in peniotron. On the other hand, they are less important if the radiation draws upon the charge bunching along the particle orbits, as in the (large orbit) gyrotron and orbitron. In the latter cases, the spatial inhomogeneities of the unperturbed motion (i.e., velocity shear) are far more important than those of the rf fields. Regardless of the dynamical properties, all of these radiation sources always operate at a frequency close to a natural frequency of the waveguide circuit.

Several interesting properties were predicted from a study of the longitudinal modes on a thin beam. For example, the orbitron configuration offers perhaps the highest small signal gain, especially at low beam energy. Away from synchronism, both the negative mass and diocotron instabilities may be stabilized by a negative radial electric field of sufficient magnitude. This arises as the electron's effective mass is changed from negative to positive. [We should stress that instability will occur if the circuit mode is synchronized with the beam mode, even if the beam has a "positive mass" behavior.] The most stable configuration against synchronous excitation and against even the resistive wall instability is when the beam is very "rigid". This occurs when the effective mass is infinite ----- i.e., when the radial electric field is adjusted so that

$$h = -\beta_o^2/2 \ .$$

All of above predictions are yet to be confirmed in controlled experiments, such as the one proposed in Fig. 16. This is essentially a two cavity klystron with a bent drift tube. The orbit is bent either by a magnetic field B_0 or by an electrostatic field, or by both. The polarity and the magnitude of the externally imposed voltage (V) and the external magnetic field B_0 may be adjusted to correspond to various values of h [Fig. 11]. The response of the electron beam may be monitored at the output cavity, after an external rf signal is impressed upon the beam at the input cavity. Such an experiment may be carried out with an electron beam of energy $\lesssim$ 10 KeV, $B_0 < 100G$, $E_0 < 5$ KeV/cm, and beam current < 0.1A. It also serves as a proof-of-principle experiment for the "super-bunched" klystron[43], as well as a controlled experiment on the orbitron mechanism discussed in this Chapter.

In the case of a thin beam, the longitudinal mode is decoupled from the transverse mode, and each mode may be treated separately. This is not the case when the beam is thick. Within a thick beam, because of the velocity shear, both Eqs. (13a) and (13b) may be satisfied for electrons at different radii. Thus, the longitudinal mode of the electrons at one layer may interact with the transverse mode of the electrons at a different layer. In fact, this was noticed in the original stability theory of the Brillouin flow, and Buneman[19] in effect already interpreted the instability as due to an exchange of the negative energy wave between those electrons satisfying (13a) with the positive energy waves of electrons at a different layer at which (13b) is satisfied! A rich amount of interesting physics buried in Eq. (30) remains to be explored.

There are deficiencies in the laminar flow model. The lack of Larmor motion in such a model was only recently corrected in the treatment of diocotron instability. Kleva, Ott and Manheimer[35] showed that the

diocotron instability cannot be completely removed from an electron sheath, regardless of the relative size between the sheath thickness and the Larmor radius. [This prevalence of the diocotron instability has recently been conjectured to occur within the Debye sheaths of a magnetized plasma and may give rise to the phenomenum of Bohm diffusion[48].]

Dynamically, perhaps the most serious deficiency in existing magnetron theories is the failure to take into account the periodic variation in the DC electric field resulting from the wall corrugation. Such a periodic variation should also be introduced in the unperturbed state of the electron flow. If one recalls the importance of the periodic motion in the mean flow of the electrons in free electron lasers, one cannot fail to worry about the possible omission of significant physics when some built-in "wiggling motions" have entirely been ignored in specifying the unperturbed state of a magnetron in virtually all existing theories .

References

1. Microwave Magnetrons, Ed. G. B. Collins (McGraw-Hill, New York, 1948)
2. Cross-Field Microwave Devices, Ed. E. Okress (Academic Press, New York, 1961) Vol. 1 and 2. These two volumes remain unsurpassed in providing broad coverage of cross-field devices. Some other useful texts are listed in Refs. 3,4.
3. M. Chodorow and C. Susskind, Fundamentals of Microwave Electronics, (McGraw Hill, New York, 1964) Chapter 10.

   R. G. Hutter, Beam and Wave Electronics in Microwave Tubes, (Van Nostrand, Princeton, NJ. 1960).

   J. F. Gittins, Power Travelling-Wave Tubes, (American Elsevier, New York, 1965).

   P. L. Kapitza, High Power Microwave Electronics, (Pergamon Press, New York, 1964) Vol. 1 and 2.
4. See e.g. R. B. Miller, Introduction to the Physics of Intense Charged Particle Beams, (Plenum, New York, 1982).
5. G. Bekefi and T. Orzechowski, Phys. Rev. Lett. 37, 379 (1976)

   A. Palevsky and G. Bekefi, Phys. Fluids 22, 986 (1979).

   A particle simulation code for relativistic magnetron was developed by A. Palevsky, doctoral dissertation, Massachusetts Institute of Technology (1980).
6. J. Benford, in this volume. An extensive amount of Soviet literature is cited there. Chapter 6 of Miller [Ref. 4] also contains a discussion of relativistic magnetrons.

7. Strictly speaking, therefore, these magnetron theories (including the present one) may be applicable only to smooth bore magnetrons, whose walls do not have corrugations. It is not clear whether the effects of wall corrugation on the unperturbed motions of the electrons would be dynamically significant.
8. See, e.g., Chapters by M. J. Baird and by V. L. Granatstein in this volume.
9. See, e.g., Chapter by J. Pasour in this volume.
10. Y. Y. Lau and L. R. Barnett, Int. J. Infrared MM waves 3, 619 (1982); also U. S. Patent No. 4550271 (issued Oct. 29, 1985).
11. G. Dohler and R. Moats, Int. Electron Device Meetings, Tech. Digest., P.400, 1978. Also, S. Ono, K. Isutaki and T. Kageyama, Int. J. Electronics 56, 507 (1984), and references therein.
12. A. Alexeff and F. Dyer, Phys. Rev. Lett. 45, 351 (1980); I. Alexeff, IEEE Trans. PS-12, 280 (1984) and Phys. Fluids 28, 1990 (1985). See, also, I.Alexeff, Chapter in this volume.
13. R. L. Walker, in P. 227 of Ref. 1.
14. E. Ott and R. V. Lovelace, Appl. Phys. Lett. 27, 378 (1975).
15. R. V. Lovelace and T. S. T. Young, Phys. Fluids 28, 2450 (1985).
16. J. Benford, Chapter in this volume.
17. This particle code, and its offsprings, are now profitably used in many applications. See, e.g., A. Drobot, Chapter in this volume.
18. G. D. Sims, P.183 in Ref. 2.
19. O. Buneman, P.380 and p.209 of Ref 2.
20. G. E. Thomas, J. Appl. Phys. 53, 3491 (1982).
21. When the number of vanes are large, it is not easy to tell whether the device operates as a peniotron or as a cyclotron maser. Experimental evidences gathered by various groups (Dohler, Barnett, Namkung) remain inconclusive at this time. See also Ref. 29 below.

22. G. Dohler, D. Gallagher, R. Moats, and F. Scafuri, Int. Electron Device Meeting, Tech. Digests. P.328 (1981).

23. W. Namkung, Phys. Fl. 27, 329 (1984). The relativistic version is given earlier by W. W. Destler et. al. Appl. Phys. Lett. 38, 570 (1981).

24. This theoretical model for orbitrons is certainly the simplest one which one can think of. Similar to the Brillouin flow in magnetrons, it should be treated as a working hypothesis. Neverthess, interesting results emerge from a study of such an idealized model. There are other more complicated theoretical models to describe the operation of orbitrons. For example, ref. 25 indicates that the TEM mode interacting with electrons with high orbital eccentricity may also lead to orbitron emission - resembling a cylindrical Backhausan oscillator. Reference 26 invoked a non-linear wave-wave coupling process.

25. J. Burke, W. M. Manheimer, and E. Ott, Phys. Rev. Lett. 56, 2625 (1986).

26. R. W. Schmacher and R. J. Harvey, Bull. Am. Phys. Soc. 29, 1179 (1984).

27. Y. Y. Lau and D. Chernin, Phys. Rev. Lett. 52, 1425 (1984).

28. D. Chernin and Y. Y. Lau, Phys. Fluids 27, 2319 (1984).

29. G. Dohler, Int. J. Electronics, 56, 617 and 629 (1984) ; P .S .Rha, L. R. Barnett, J. M. Baird and R. W. Grow, Int. Electron Device Meet. Tech. Digest, p.525 (1985), U. A. Shrivastava, R. W. Grow, P. S. Rha, J. M. Baird and L. R. Barnett, Int. J. Electron., Vol. 61, p.33 (1986). P. Vitello, IEEE Trans. Vol. MTT-32, p. 917 (1984); also, to be published. W. Namkung, to be published.

30. G. C. MacFarlane and H. G. Hay, Phys. Soc. (Londan) Proceedings, (1950); O. Buneman, J. Electron Control 3, 507 (1957); R. L. Kyhle and H. F. Webster, IRE Trans. Electron Devices. ED-3, 172 (1956); J. R. Pierce ibid., P.183; R. H. Levy, Phys. Fluids. 8, 1288 (1965); O. Buneman, R. H. Levy and L. M. Linson, J. Appl. Phys. 37, 3203 (1966), V. K. Neil and W. Heckrotte, J. Appl. Phys. 36, 2761 (1965); R. W. Gould, ibid, 28, 599 (1957). See also J. D. Lawson, The Physics of Charged Partical Beams (Clarendon, Oxford, 1977).

31. O. Buneman, in Ref. 2, P.367.

32. G. Mourier, in Ref. 2, P.396.

33. R. C. Davidson, Theory of Non-Neutral Plasmas. (Benjamin, New York, 1974); H. S. Uhm and J. G. Siambis, Phys. Fluids 22, 2377 (1979) and references therein.

34. See, e.g., Chapter 6 of Gittins and Chapter 10 of Chodorow and Susskind, Ref. 3.

35. R. G. Kleva, E. Ott and W. M. Manheimer, Phys. Fluids. 28, 941 (1985).

36. Y. Y. Lau, IEEE Trans. Vol. ED-29, 320 (1982), and Vol. ED-31, 329 (1984).

37. See, e.g., S. Chandrasekhar, Hydrodynamic and Hydromagnetic Stability, (Oxford University Press, New York), 1960; C. C. Lin, Theory of Hyrodynamic Stability, (Cambridge University Press, London), 1955; and P. G. Drazin and L. N. Howard, Adv. Appl. Mech. 9,1 (1966)

38. J. L. Hirshfield and J. M. Wachtel, Phys. Rev. Lett. 12, 533 (1964).

39. The equilibrium quantities h, E_o and B which appear in Eqs. (15), (16) and elsewhere in the text [e.g., in the dispersion relations (25) and (31)] actually include the DC self fields. It turns out that, for a thin beam, the DC self field modifies the dispersion relation (25) only by introducing the extra term proportional to $(\tau/R)^2$ in (31). See Refs. (27), (28) for more detail.

40. R. J. Briggs and V. K. Neil, Plasma Physics 9, 209 (1967).

41. G. Dohler and W. Fritz, Int. J. Electronics, 55, 505, 523 (1983).

42. C. E. Nielsen, A. M. Sessler, and K. R. Symon, in Proc. Int. Conf. High-Energy Accelerators and instrumentation (Geneva, Switzerland), Geneva: CERN, P. 239, 1959.

A. A. Kolomenskii and A. N. Lebedev, ibid, P. 115;

Also, R. W. Landau and V. K. Neil, Phys. Fluids 9, 2412 (1966).

43. Y. Y. Lau, Phys. Rev. Lett. 53, 395 (1984).

44. L. J. Laslett, V. K. Neil and A. M. Sessler, Rev. Scient. Inst. 36, 436 (1965) and references therein.

45. A. M. Sessler, private communication (1983).

46. I. Alexeff (private communication, 1984) also alerted us of this possibility.

47. Y. Y. Lau and R. J. Briggs, Phys. Fluids 14, 967 (1971).

48. Y. Y. Lau, Naval Research Laboratory, Memo Report No. 5968 (April 1987).

A Note on Bohm Difusion

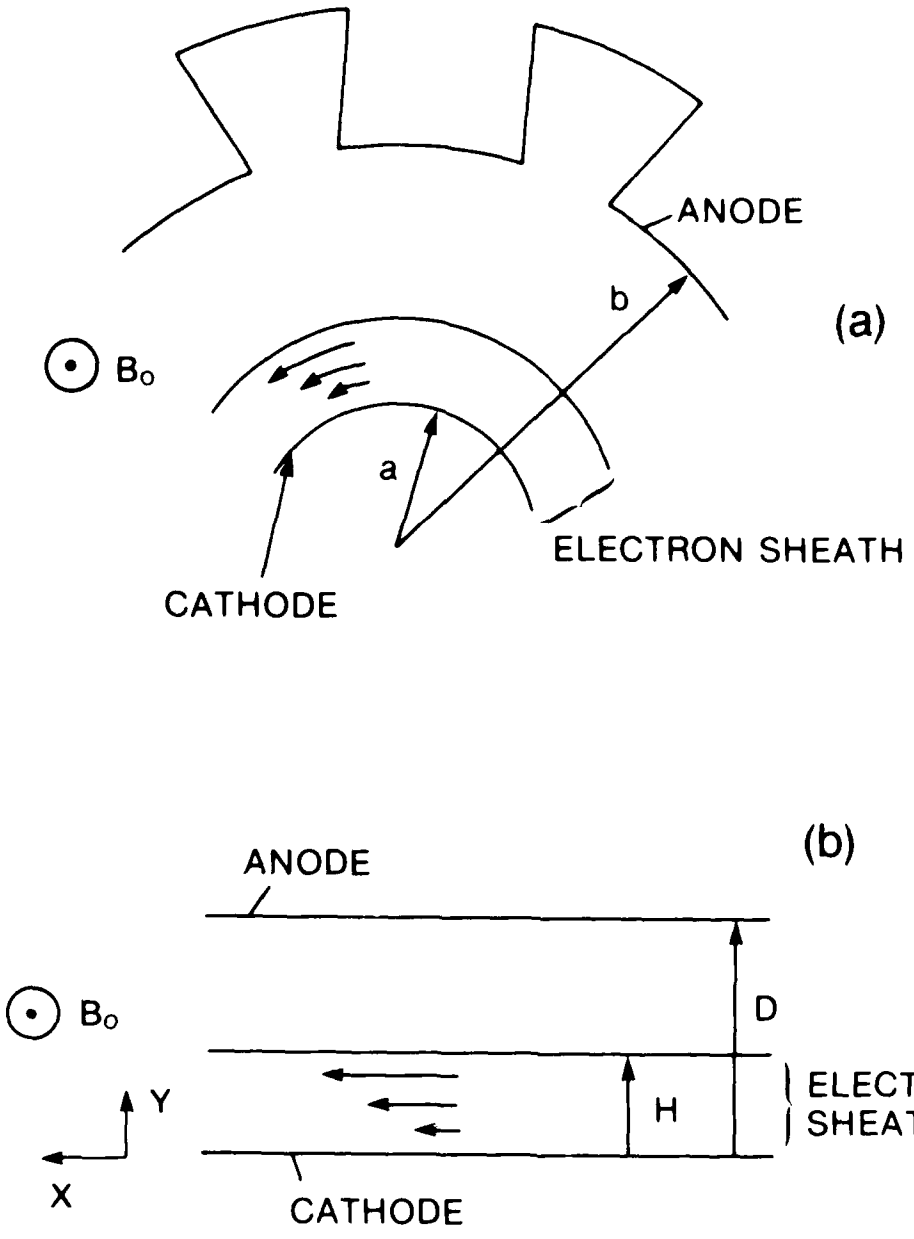

Fig. 1 (a). Laminar flow model of magnetron.

(b). Further idealization.

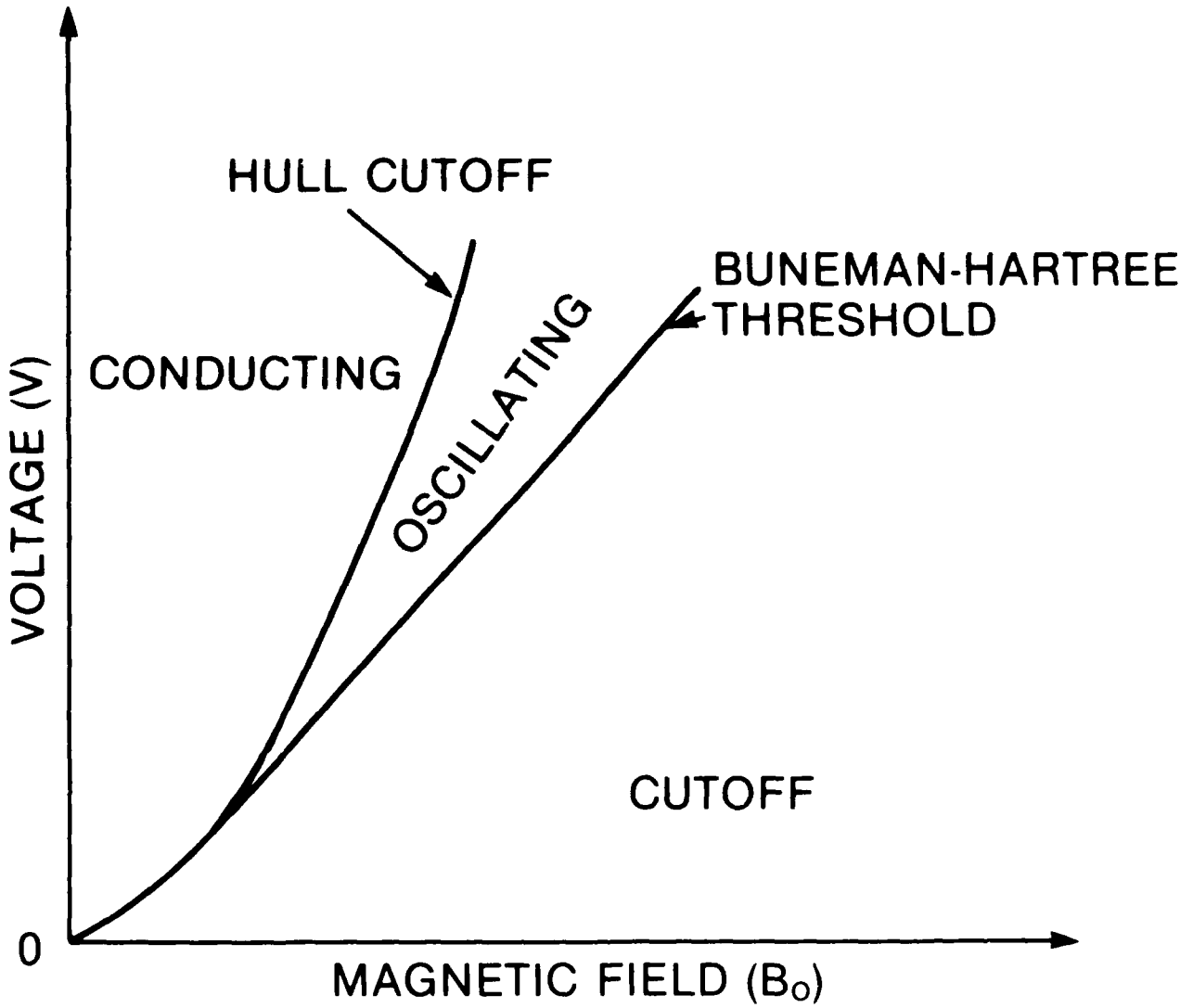

Fig. 2 The Hull cut-off voltage and the Buneman-Hartree threshold voltage. The latter curve is tangent to the former.

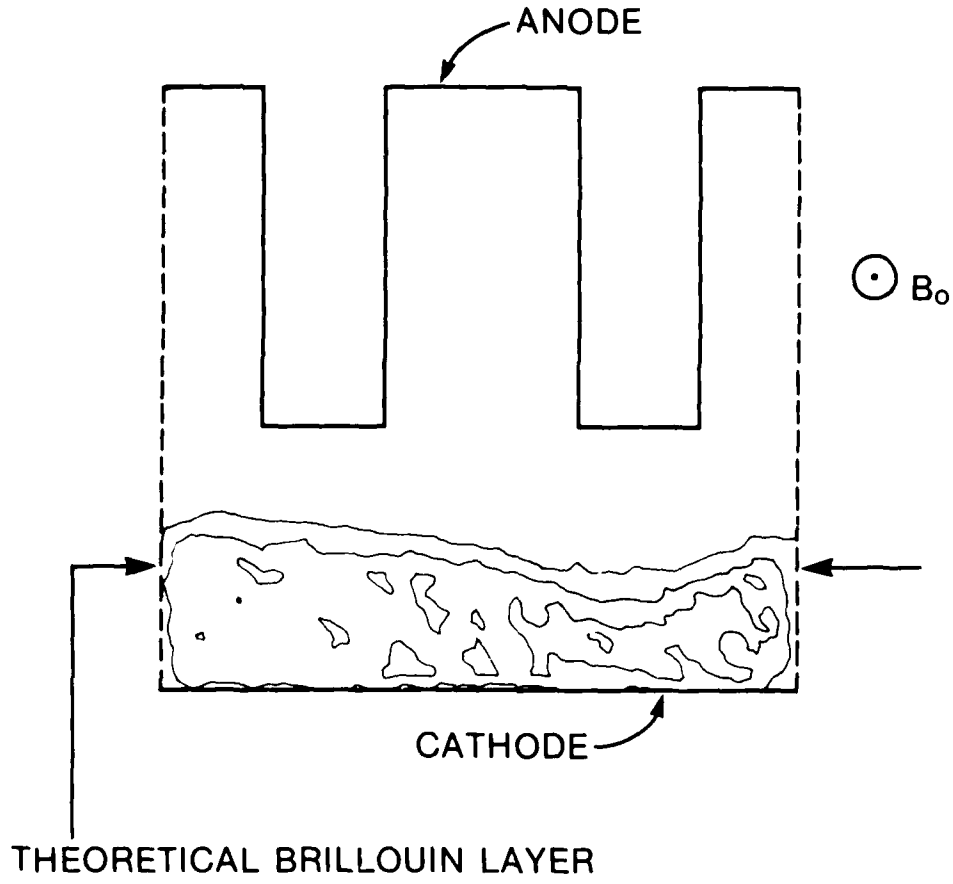

Fig. 3 Density contours obtained from Palevsky's particle simulation [Ref. 5] during the early stage. The arrows indicate the theoretical Brillouin layer.

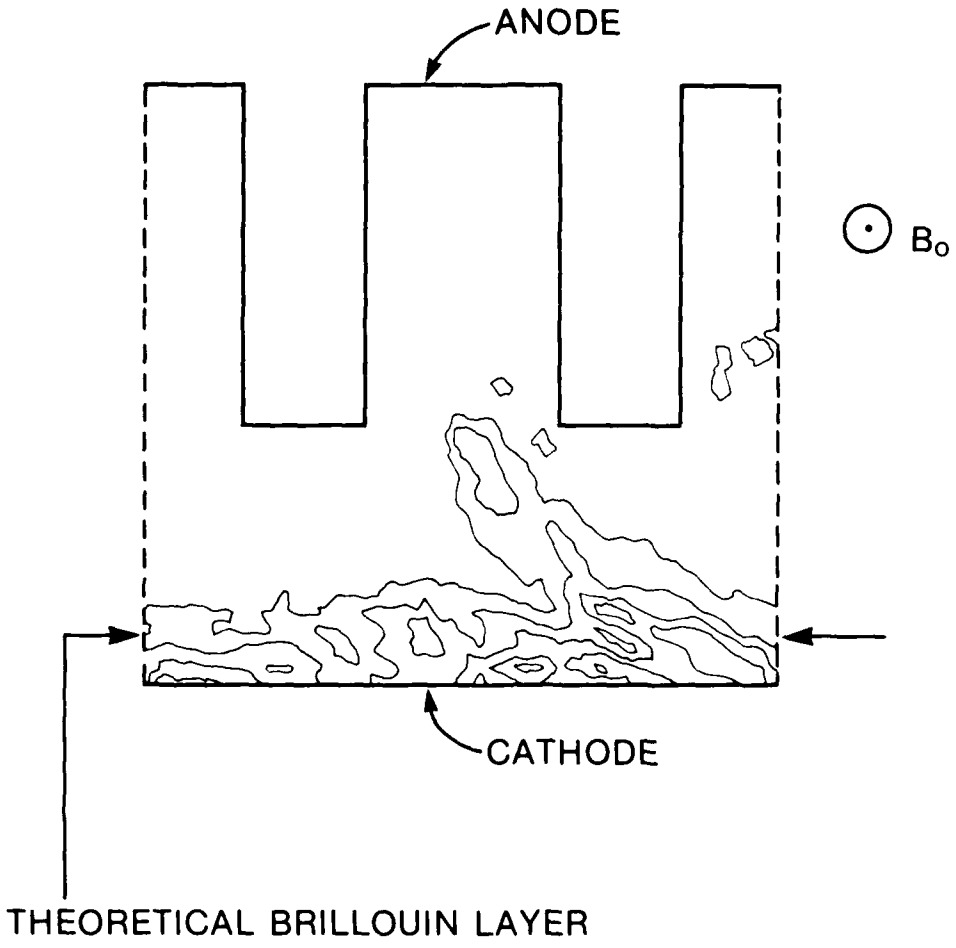

Fig. 4 Same as in Fig. 3, but at a later stage when oscillation is fully developed. The magnetron voltage is reduced, leading to a narrower Brillouin sheath as shown in this figure.

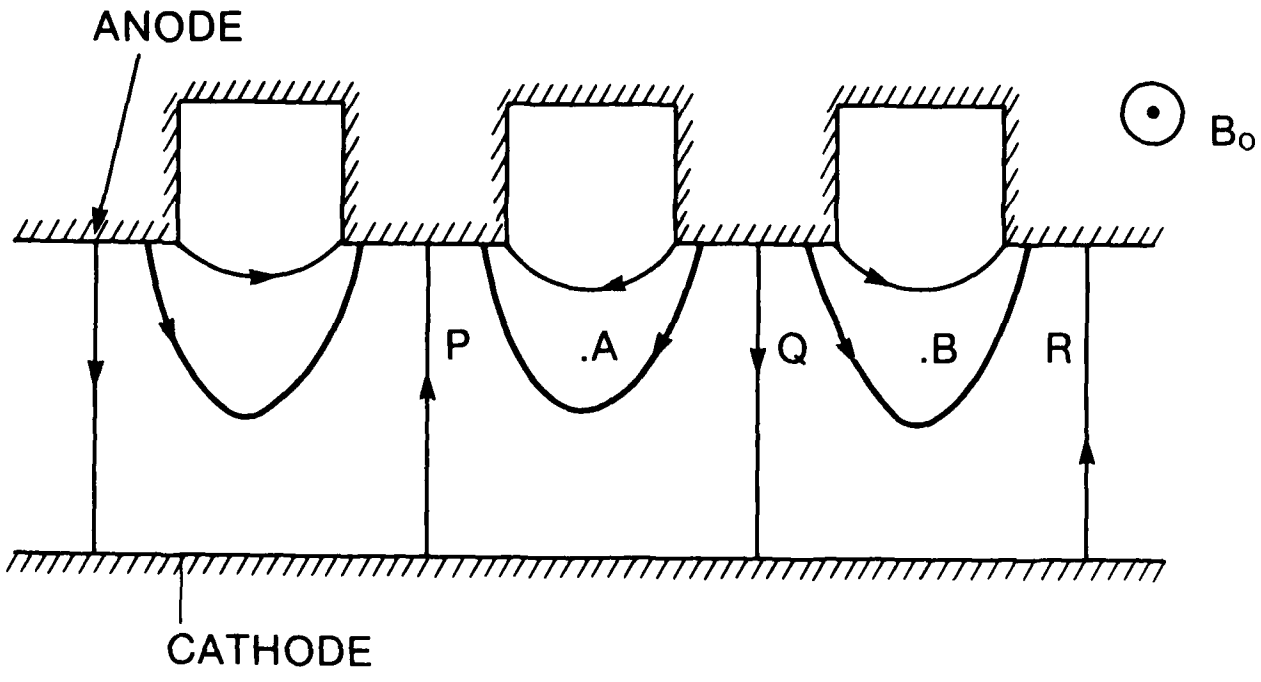

Fig. 5 A planar magnetron model and the rf electric fields of the pi-mode.

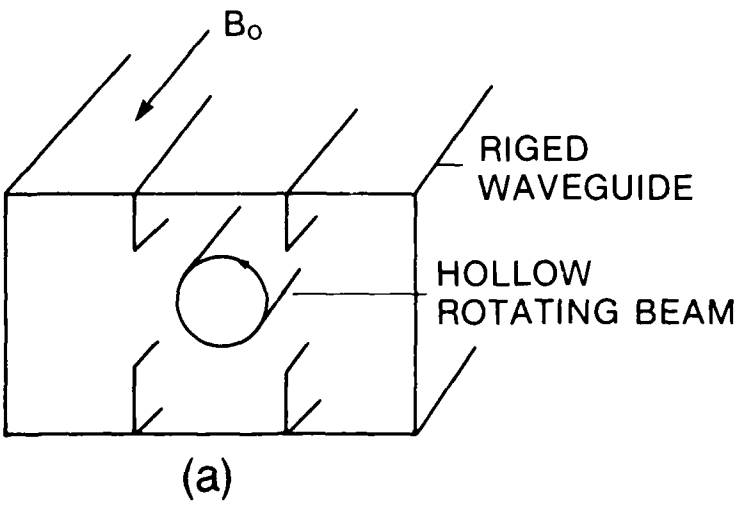

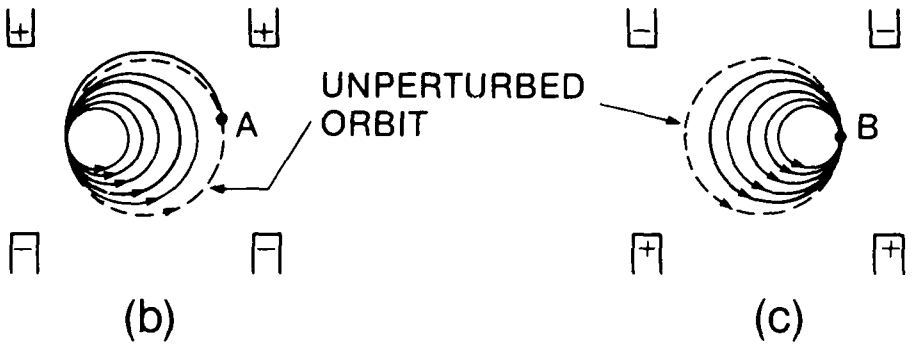

Fig. 6 (a) A peniotron model.

(b)(c) Action of the rf electric field on electron A which is initially in an accelerating phase and on electron B which is initially in a decelerating phase. The dotted circles denote the unperturbed orbits.

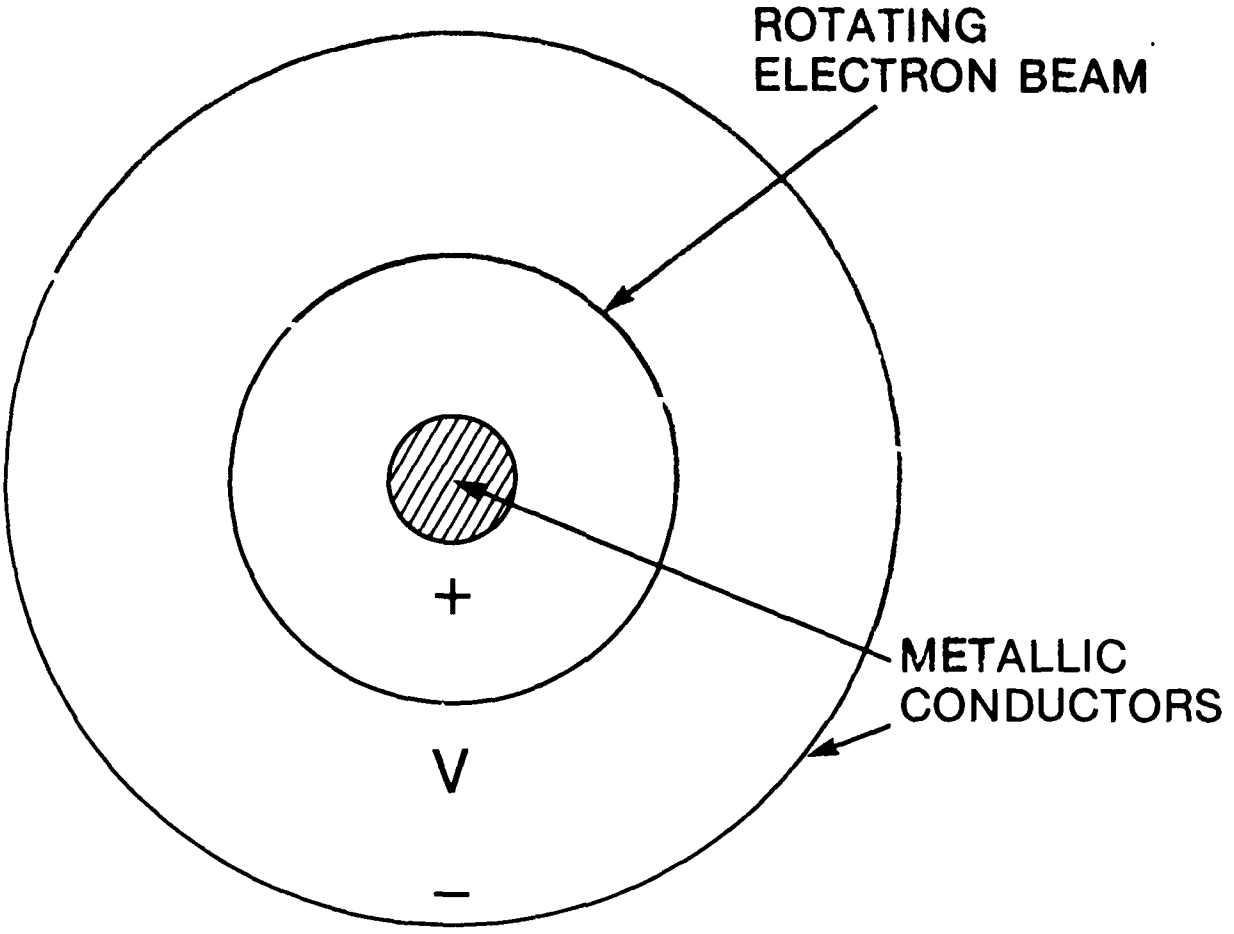

Fig. 7 An orbitron model. The electron layer rotates about the center conductor under a radial electric field. This model is used in Refs. (12, 27, 28).

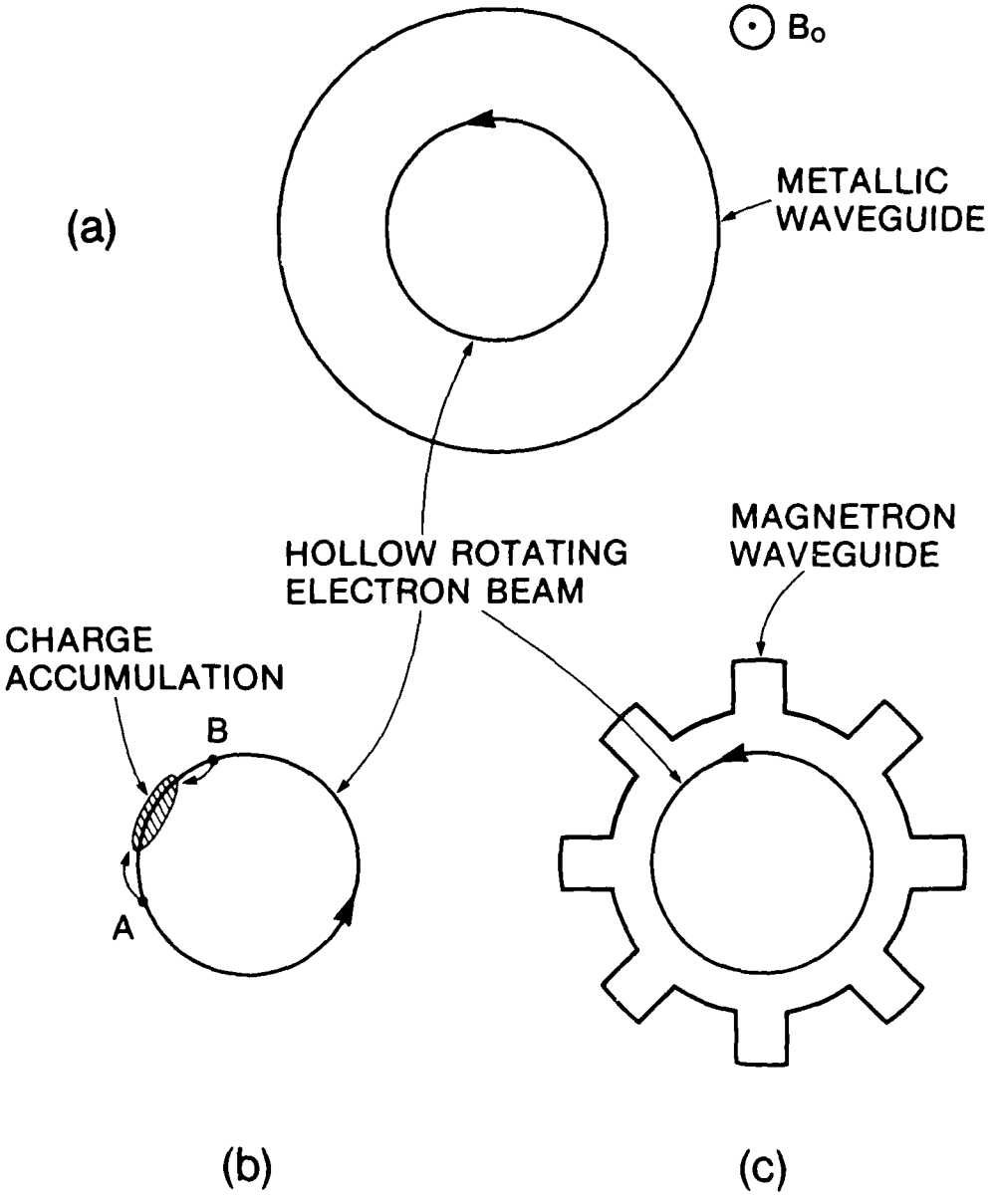

Fig. 8 (a) A gyrotron model.

(b) Negative mass effect.

(c) A gyromagnetron model. A magnetron waveguide is used to encourage harmonic generation.

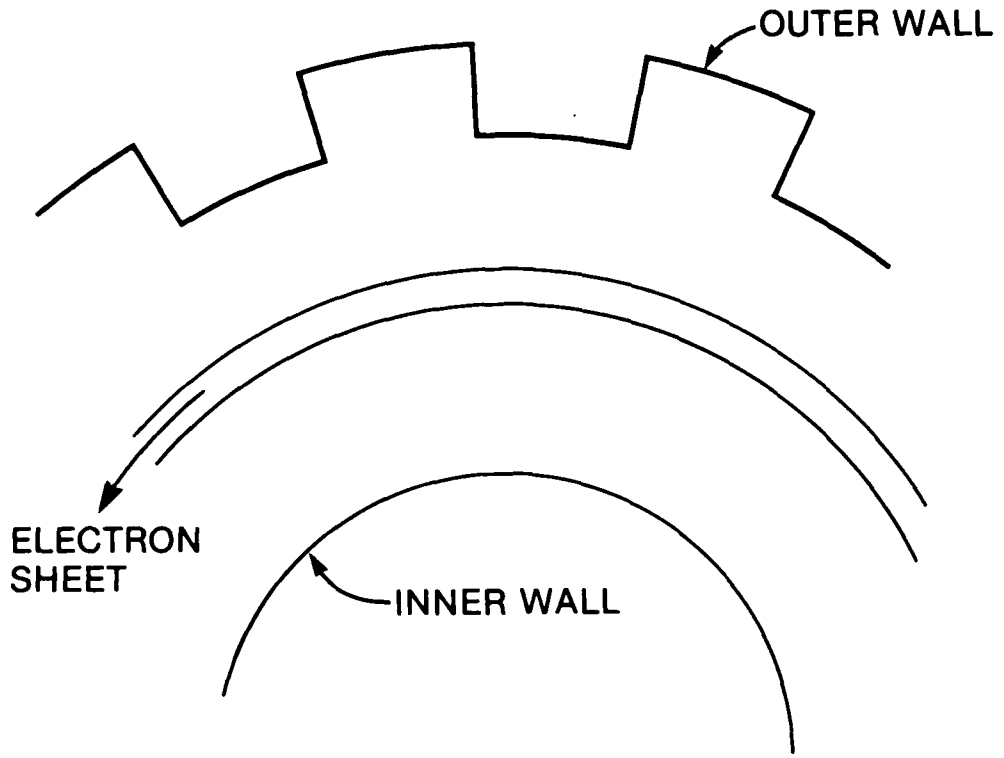

$$\vec{E}_o = \hat{r}\, E_o(r)$$

$$\vec{B}_o = \hat{z}\, B_o(r)$$

Fig. 9 A model for which a simple dispersion relation can be obtained analytically. It is representative of cross field devices, gyrotron, orbitron, peniotron, gyromagnetron, depending on the circuits and on the magnitude and polarity of E_o and B_o.

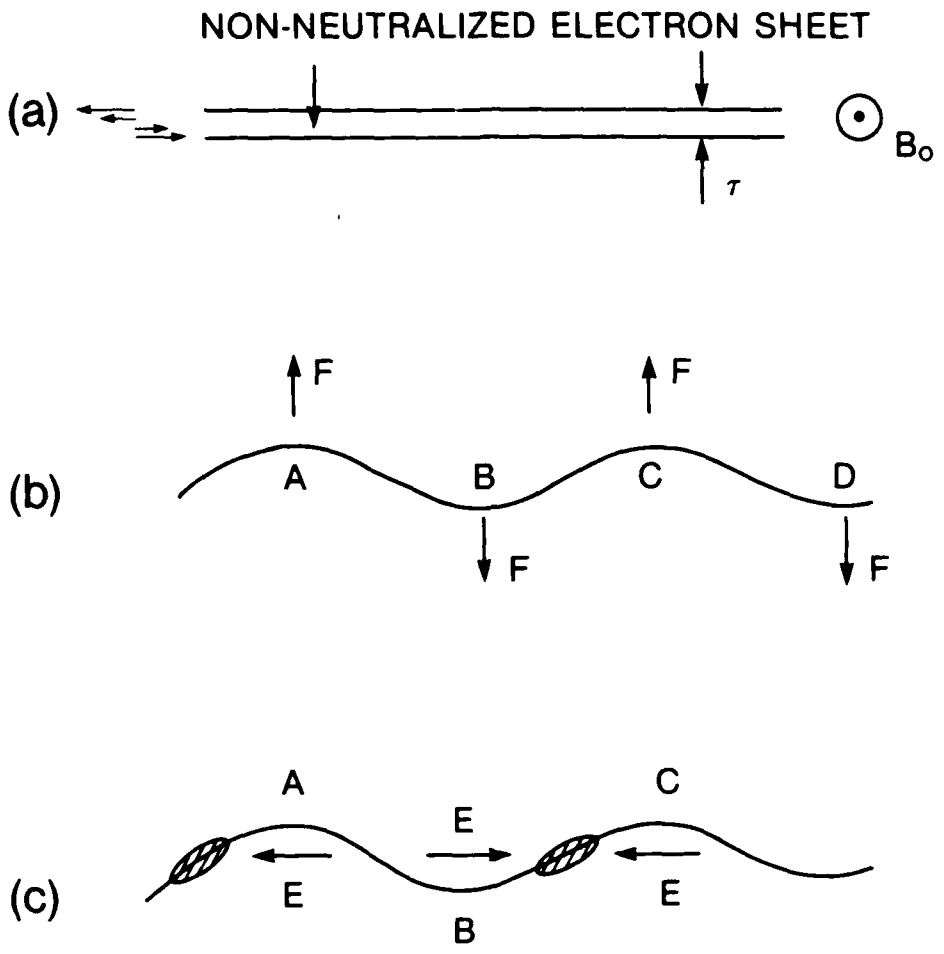

Fig.10 Physical origin of the diocotron instabilities, viewed in the rest frame of the mean flow:
(a) velocity shear generated by the electron self field.
(b)(c) ripple on the sheet and its reinforcement.

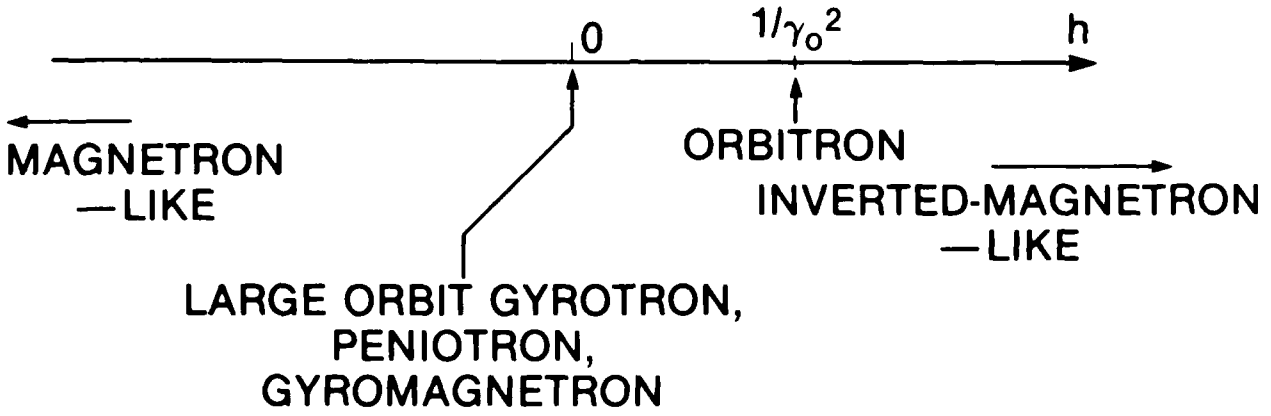

Fig.11 Correspondence between the values of the normalized electric field h and the various types of equilibrium.

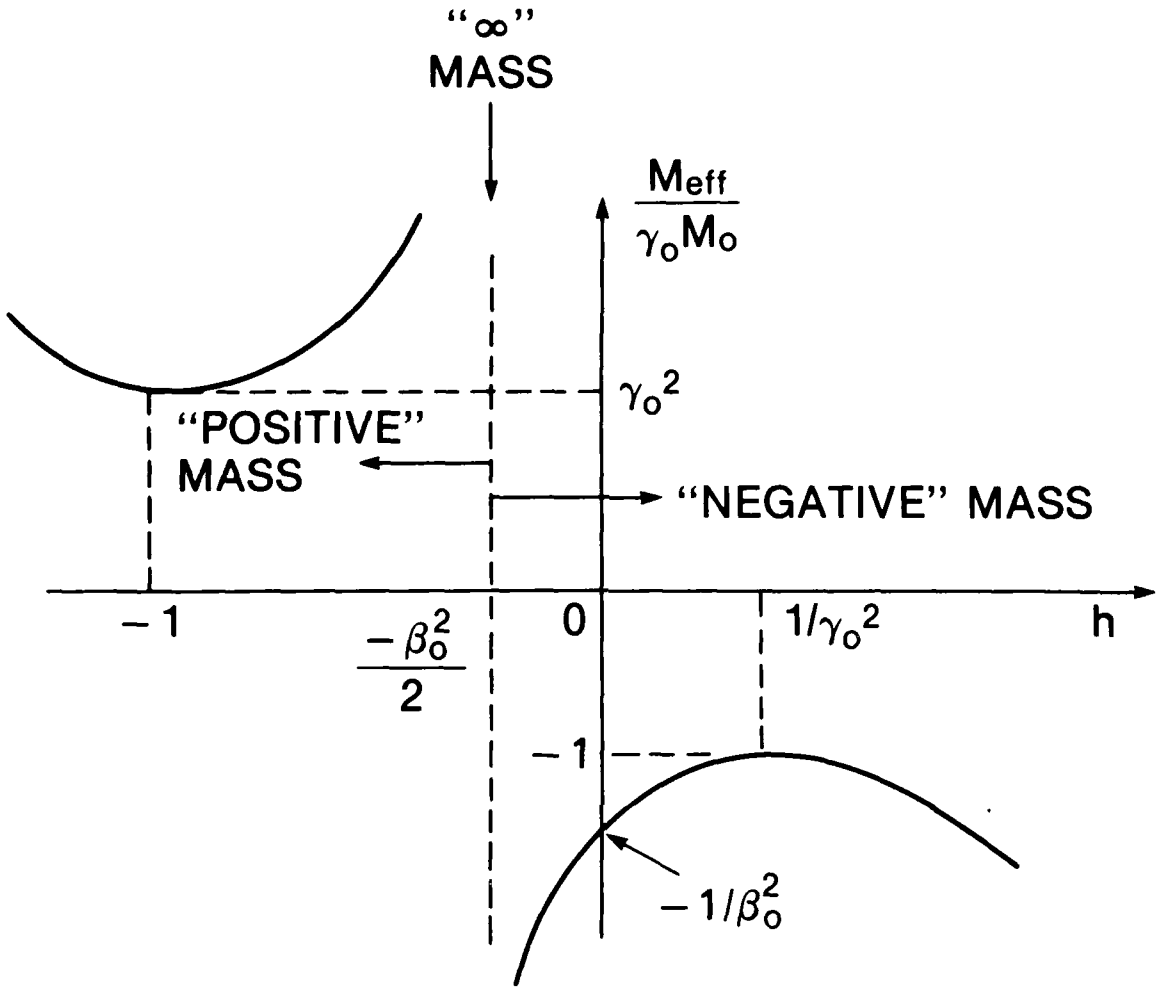

Fig.12 The normalized effective mass $M_{eff}/\gamma_o m_o$ as a function of h. Compare with Fig. 11.

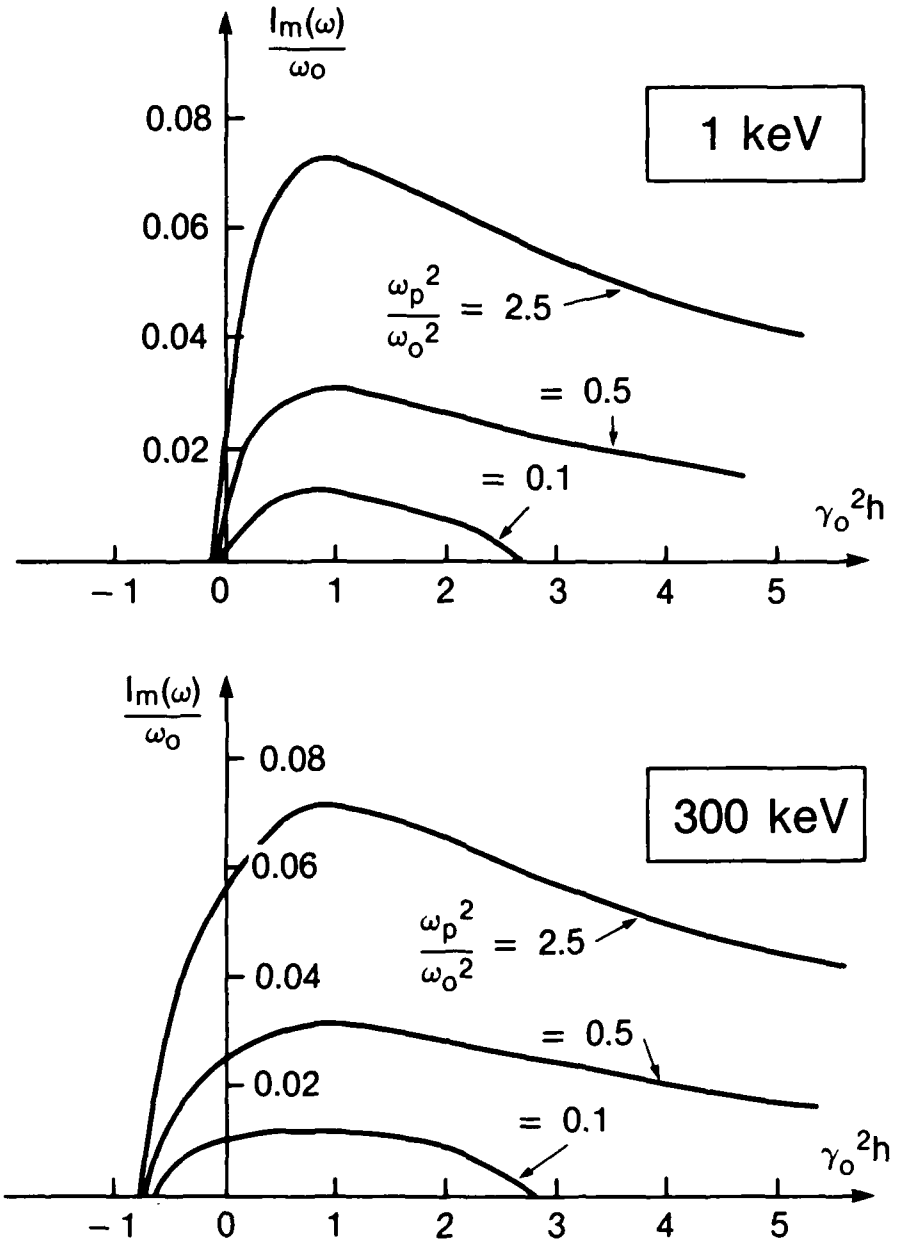

Fig.13 Growth rates of longitudinal modes in a thin electron layer as a function of the equilibrium type (h), at both non-relativistic energy (top) and relativistic energy (bottom). They are calculated from (31) with ℓ =1, τ/R=0.016, b_+=5, b_-=3, and beam kinetic energy and density as specified in the figure.

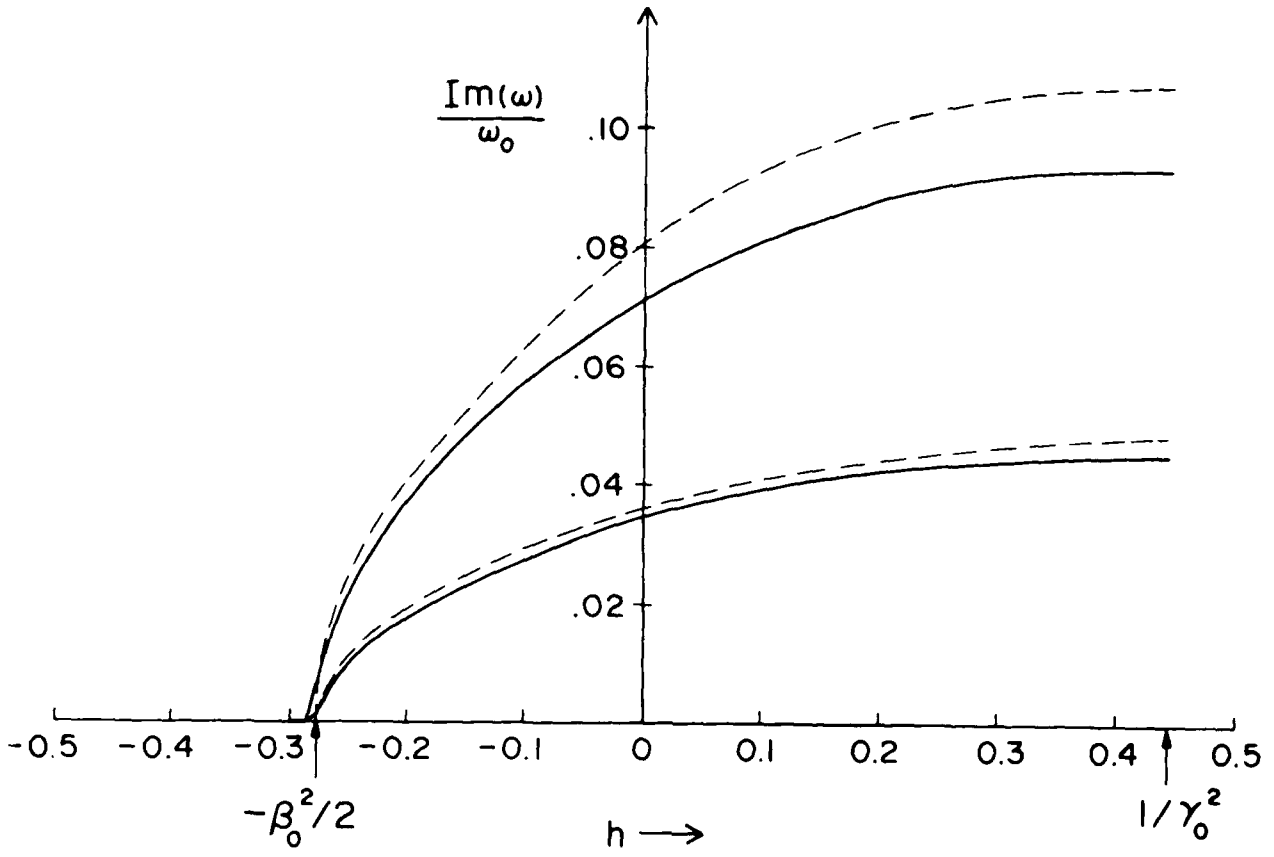

Fig.14 Normalized growth rate for longitudinal modes as a function of h for a test case with a = 0.6m, b=2.6m, R = 1.0m, $\tau/R = 0.02$, $\gamma_o = 1.5$, $\ell = 1$. (a being the inner wall radius and b being the outer wall radius). A solid curve indicates data obtained from a numerical solution of Eq. (30); the dashed line is a plot of Eq. (31). The upper pair of curves is for $\nu/\gamma_o = 7.88 \times 10^{-3}$, $\omega_p^2/\omega_o^2 = 1.42$, the lower pair is for $\nu/\gamma_o = 1.57 \times 10^{-3}$, $\omega_p^2/\omega_o^2 = 0.28$.

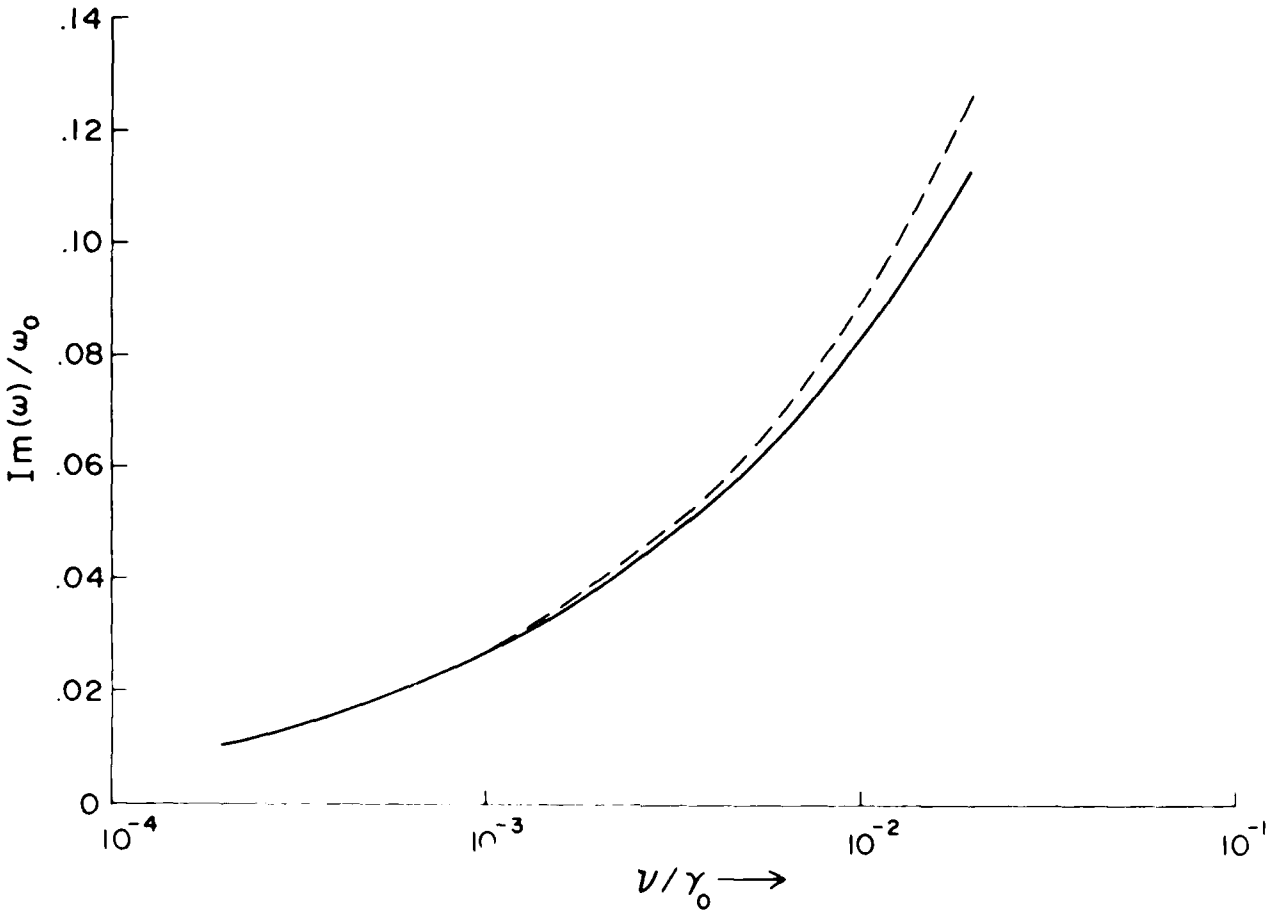

Fig. 15 Normalized growth rate for the longitudinal modes versus ν/γ_0 for a test case : a=0.5m, b=2.2m, r_1=0.99m, r_2=1.01m, γ_0=3, ℓ =1. A solid curve denotes data obtained from a numerical solution of the eigenvalue problem (30); a dashed curve denotes data from the dispersion relation, Eq. (31).

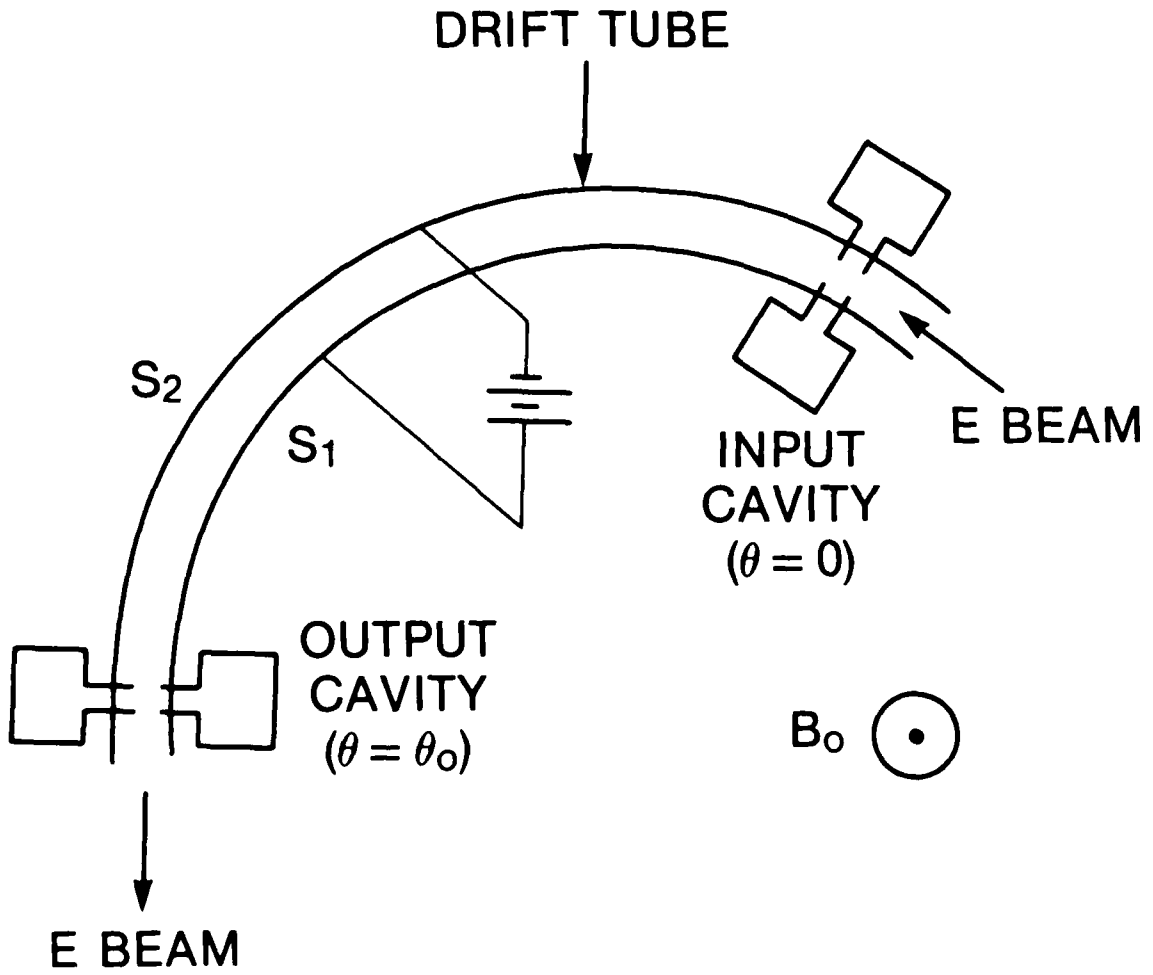

Fig.16 A schematic drawing of a proposed laboratory experiment which may demonstrate the effects of equilibrium type on the dynamical properties of an electron beam. Parameters required : Beam energy < 10KeV, current <0.1A, radial electric field E_0 < 5KeV/cm, B_0 < 100G.

DISTRIBUTION LIST*

Naval Research Laboratory
4555 Overlook Avenue, S.W.
Washington, DC 20375-5000

Attn: Code 1000 - Commanding Officer, CAPT William C. Miller
1001 - Dr. T. Coffey
1005 - Head, Office of Management & Admin.
1005.6 - Head, Directives Staff
1220 - Mr. M. Ferguson
2000 - Director of Technical Services
2604 - NRL Historian
2628 - Documents (22 copies)
2634 - D. Wilbanks
4000 - Dr. W. R. Ellis
4600 - Dr. D. Nagel
4603 - Dr. W.W. Zachary
4700 - Dr. S. Ossakow (26 copies)
4700.1 - Dr. M. Friedman
4710 - Dr. J.A. Pasour
4710 - Dr. C.A. Kapetanakos
4730 - Dr. R. Elton
4730 - Dr. B. Ripin
4740 - Dr. W.M. Manheimer
4740 - Dr. S. Gold
4790 - Dr. P. Sprangle (10 copies)
4790 - Dr. C.M. Tang (5 copies)
4790 - Dr. M. Lampe (5 copies)
4790 - Dr. Y.Y. Lau (100 copies)
4790 - Dr. G. Joyce
4790 - Dr. T. Godlove
4790A- W. Brizzi
6840 - Dr. S.Y. Ahn
6840 - Dr. A. Ganguly
6840 - Dr. R.K. Parker
6843 - Dr. N.R. Vanderplaats
6875 - Dr. R. Wagner

* Every name listed on distribution gets one copy except for those where extra copies are noted.

Prof. I. Alexeff (3 copies)
Dept. of Electrical Engineering
University of Tennessee
Knoxville, TN 37996-2100

Dr. Bruce Anderson
Lawrence Livermore National Laboratory
L-436
P. O. Box 808
Livermore, CA 94550

Dr. T. Antonsen
University of Maryland
College Park, MD 20742

Assistant Secretary of the
Air Force (RD&L)
Room 4E856, The Pentagon
Washington, D.C. 20330

Dr. W. A. Barletta
Lawrence Livermore National Lab.
P. O. Box 808
Livermore, CA 94550

Dr. L. R. Barnett
3053 Merrill Eng. Bldg.
University of Utah
Salt Lake City UT 84112

Dr. Robert Behringer
Office of Naval Research
1030 E. Green
Pasadena, CA 91106

Dr. G. Bekefi (2 copies)
Mass. Institute of Tech.
Bldg. 26
Cambridge, MA 02139

Prof. Herbert Berk
Institute for Fusion Studies
University of Texas
Austin, TX 78712

Dr. T. Berlincourt
Office of Naval Research
Attn: Code 420
Arlington, VA 22217

Dr. I. B. Bernstein
Mason Laboratory
Yale University
400 Temple Street
New Haven, CT 06520

Prof. A. Bers
Dept. of Electrical Engineering
MIT
Cambridge, MA 02139

Prof. Charles K. Birdsall
Dept. of Electrical Engineering
University of California
Berkeley, CA 94720

Dr. H. Brandt (3 copies)
Department of the Army
Harry Diamond Laboratory
2800 Powder Mill Rd.
Adelphi, MD 20783

Dr. Charles Brau (2 copies)
Los Alamos National Scientific
Laboratory
P.O. Box 1663, M.S. - 817
Los Alamos, NM 87545

Dr. R. Briggs (3 copies)
Lawrence Livermore National Lab.
Attn: (L-71)
P.O. Box 808
Livermore, CA 94550

Prof. O. Buneman
ERL, Stanford University
Stanford, CA 94305

Dr. K. J. Button
Francis Bitter Natl. Magnet Lab.
Mass. Institute of Technology
Cambridge, MA 02139

Dr. J. A. Byers
Lawrence Livermore National Lab.
Attn: (L-630)
P. O. Box 808
Livermore, CA 94550

Prof. J. D. Callen
Nuclear Engineering Dept.
University of Wisconsin
Madison, WI 53706

Dr. Malcolm Caplan
4219 Garland Drive
Fremont, CA 94536

Dr. Maria Caponi
TRW, Building R-1, Room 1184
One Space Park
Redondo Beach, CA 90278

Prof. Frank Chan
School of Eng. & Applied Sciences
Univ. of Calif. at Los Angeles
7731 K Boelter Hall
Los Angeles, CA 90024

Dr. V. S. Chan
GA Technologies
P.O. Box 85608
San Diego, CA 92138

Dr. D. P. Chernin (3 copies)
Science Applications Intl. Corp.
1720 Goodridge Drive
McLean, VA 22102

Prof. M. V. Chodorow
Ginzton Laboratory
Stanford, University
Stanford, CA 94305

Dr. William Colson
Berkeley Research Asso.
P. O. Box 241
Berkeley, CA 94701

Dr. William Condell
Office of Naval Research
Attn: Code 421
800 N. Quincy St.
Arlington, VA 22217

Dr. Richard Cooper
Los Alamos National Scientific
Laboratory
P.O. Box 1663
Los Alamos, NM 87545

Prof. B. Coppi
Dept. of Physics, 26-217
MIT
Cambridge, MA 02139

Dr. Bruce Danly
MIT
NW16-174
Cambridge, MA 02139

Dr. R. Davidson
Plasma Fusion Center
Mass. Institute of Tech.
Cambridge, MA 02139

Dr. John Dawson
Physics Department
University of California
Los Angeles, CA 90024

Dr. David A. G. Deacon
Deacon Research
Suite 203
900 Welch Road
Palo Alto, CA 94306

Defense Tech. Information Ctr.
Cameron Station
5010 Duke Street
Alexandria, VA 22314

Deputy Under Secretary of
Defense for R&AT
Room 3E114, The Pentagon
Washington, D.C. 20301

Dr. W. W. Destler
Dept. of Electrical Engineering
University of Maryland
College Park, MD 20742

Prof. P. Diament
Dept. of Electrical Engineering
Columbia University
New York, NY 10027

Director of Research (2 copies)
U. S. Naval Academy
Annapolis, MD 21402

Dr. Gunter Dohler (3 copies)
Northrop Corporation
Defense Systems Division
600 Hicks Road
Rolling Meadows, IL 60008

Dr. Franklin Dolezal
Hughes Research Laboratory
3011 Malibu Canyon Rd.
Malibu, CA 90265

Dr. A. Drobot
Science Applications Intl. Corp.
1710 Goodridge Road
McLean, VA 22102

Dr. Dwight Duston
Strategic Defense Initiative Org.
OSD/SDIO/IST
Washington, DC 20301-7100

Dr. Luis R. Elias
Quantum Institute
University of California
Santa Barbara, CA 93106

Dr. W. Fawley
L-626
Lawrence Livermore National Laboratory
P. O. Box 808
Livermore, CA 94550

Dr. F. S. Felber
JAYCOR
2055 Whiting Street
Suite 500
Alexandria, VA 22304

Dr. H. Fleischmann
Cornell University
Ithaca, NY 14850

Dr. Lazar Friedland
Dept. of Eng. & Appl. Science
Yale University
New Haven, CT 06520

Dr. R. Gajewski
Div. of Advanced Energy Projects
U. S. Dept of Energy
Washington, DC 20545

Dr. Richard L. Garwin
IBM, T. J. Watson Research Ctr.
P.O. Box 218
Yorktown Heights, NY 10598

Prof. Ward Getty
University of Michigan
Ann Arbor, MI 53706

Prof. Ronald Gilgenbach (3 copies)
Dept. Nucl. Engineering
University of Michigan
Ann Arbor, MI 48109

Dr. B. B. Godfrey
Mission Research Corporation
1400 San Mateo, S.E.
Albuquerque, NM 87108

Dr. C. Grabbe
Department of Physics
University of Iowa
Iowa City, Iowa 52242

Dr. V. L. Granatstein (3 copies)
Dept. of Electrical Engineering
University of Maryland
College Park, MD 20742

Dr. R. Harvey
Hughes Research Laboratory
3011 Malibu Canyon Road
Malibu, CA 90265

Prof. Herman A. Haus
Mass. Institute of Technology
Rm. 36-351
Cambridge, MA 02139

Dr. Fred Hopf
Optical Sciences Building, Room 602
University of Arizona
Tucson, AZ 85721

Dr. G. L. Johnston
NW 16-232
Mass. Institute of Tech.
Cambridge, MA 02139

Dr. Shayne Johnston
Physics Department
Jackson State University
Jackson, MS 39217

Dr. Howard Jory
Varian Associates, Bldg. 1
611 Hansen Way
Palo Alto, CA 94303

Prof. Terry Kammash
University of Michigan
Ann Arbor, MI 53706

Prof. Donald Kerst
3291 Chamberlin Hall
University of Wisconsin
Madison, WI 53706

Dr. K. J. Kim, MS-101
Lawrence Berkeley Lab.
Rm. 223, B-80
Berkeley, CA 94720

Dr. A. Kolb
Maxwell Laboratories, Inc.
8835 Balboa Avenue
San Diego, CA 92123

Prof. N. M. Kroll
Department of Physics
B-019, UCSD
La Jolla, CA 92093

Dr. S. P. Kuo
Polytechnic Institute of NY
Route 110
Farmingdale, NY 11735

Dr. Thomas Kwan
Los Alamos National Scientific
Laboratory, MS608
P. O. Box 1663
Los Alamos, NM 87545

Dr. Willis Lamb
Optical Sciences Center
University of Arizona
Tucson, AZ 87521

Dr. Rulon K. Linford
CTR-11, Mail Stop: 646
Los Alamos National Laboratory
P. O. Box 1663
Los Alamos, NM 87545

Dr. John Madey
S.P.R.C.
Physics Department
Stanford University
Stanford, CA 94305

Dr. S. A. Mani
W. J. Schafer Assoc., Inc.
10 Lakeside Office Park
Wakefield, MA 01880

Dr. J. Mark
Lawrence Livermore National Lab.
Attn: L-477
P. O. Box 808
Livermore, CA 94550

Dr. W. E. Martin
L-436
Lawrence Livermore National Lab.
P. O. Box 808
Livermore, CA 94550

Dr. John McAdoo
Dept. of Electrical Engineering
University of Maryland
Relocatable Classroom, Bldg. 335
College Park, MD 20742

Prof. George Morales
Dept. of Physics
U.C.L.A.
Los Angeles, CA 90024

Dr. Philip Morton
Stanford Linear Accelerator Center
P.O. Box 4349
Stanford, CA 94305

Dr. J. Nation
Cornell University
Ithaca, NY 14850

Dr. Kelvin Neil
Lawrence Livermore National Lab.
Code L-321, P.O. Box 808
Livermore, CA 94550

Dr. T. Orzechowski
L-436
Lawrence Livermore National Lab.
P. O. Box 808
Livermore, CA 94550

Prof. E. Ott
Department of Physics
University of Maryland
College Park, MD 20742

Dr. Robert B. Palmer
Brookhaven National Laboratories
Associated Universities, Inc.
Upton, L.I., NY 11973

Dr. Richard H. Pantell
Stanford University
Stanford, CA 94305

Dr. Dennis Papadopoulos
Astronomy Department
University of Maryland
College Park, Md. 20742

Dr. R. R. Parker
NW16-288
Plasma Fusion Center
MIT
Cambridge, MA 02139

Dr. C. K. N. Patel
Bell Laboratories
Murray Hill, NJ 07974

Dr. Richard M. Patrick
AVCO Everett Research Lab., Inc.
2385 Revere Beach Parkway
Everett, MA 02149

Dr. Claudio Pellegrini
Brookhaven National Laboratory
Associated Universities, Inc.
Upton, L.I., NY 11973

Dr. Sam Penner
National Bureau of Standards,
RADP B102
Washington, DC 20234

Dr. Hersch Pilloff
Code 421
Office of Naval Research
Arlington, VA 22217

Dr. Donald Prosnitz
Lawrence Livermore National Lab.
Attn: L-470
P. O. Box 808
Livermore, CA 94550

Dr. M. Reiser
University of Maryland
Department of Physics
College Park, MD 20742

Dr. S. Ride
Johnson Space Center
Houston, TX 77058

Dr. C. W. Roberson (5 copies)
Code 412
Office of Naval Research
800 N. Quincy Street
Arlington, VA 22217

Dr. Marshall N. Rosenbluth
Institute for Fusion Studies
The Univ. of Texas at Austin
Austin, TX 78712

Dr. N. Rostoker
University of California
Department of Physics
Irvine, CA 92717

Dr. J. Scharer
ECE Dept.
Univ. of Wisconsin
Madison, WI 53706

Dr. E. T. Scharlesmann
L626
Lawrence Livermore National Laboratory
P. O. Box 808
Livermore, CA 94550

Dr. Michael Schlesinger
ONR Code 1112
800 N. Quincy Street
Arlington, VA 22217-5000

Prof. S. P. Schlesinger
Dept. of Electrical Engineering
Columbia University
New York, NY 10027

Dr. Howard Schlossberg
AFOSR
Bolling AFB
Washington, D.C. 20332

Dr. George Schmidt
Stevens Institute of Technology
Physics Department
Hoboken, NJ 07030

Dr. H. Schwettmann
Phys. Dept. & High Energy
Physics Laboratory
Stanford University
Stanford, CA 94305

Dr. Marlan O. Scully
Dept. of Physics & Astronomy
Univ. of New Mexico
800 Yale Blvd. NE
Albuquerque, NM 87131

Dr. A. M. Sessler
Lawrence Berkeley Laboratroy
University of California
1 Cyclotron Road
Berkeley, CA 94720

Dr. W. Sharp
L-626
Lawrence Livermore National Laboratory
P. O. Box 808
Livermore, CA 94550

Dr. R. Shefer
Science Research Laboratory
15 Ward Street
Somerville, MA 02143

Dr. Shen Shey (2 copies)
DARPA/DEO
1400 Wilson Boulevard
Arlington, VA 22209

Dr. D. J. Sigmar
Oak Ridge National Laboratory
P. O. Box Y
Oak Ridge, TN 37830

Dr. J. S. Silverstein
Harry Diamond Laboratories
2800 Powder Mill Road.
Adelphi, MD 20783

Dr. Jack Slater
Spectra Technology
2755 Northup Way
Bellevue, WA 98004

Dr. Lloyd Smith
Lawrence Berkeley Laboratory
University of California
1 Cyclotron Road
Berkeley, CA 94720

Dr. R. Sudan
Cornell University
Ithaca, NY 14850

Dr. David F. Sutter
ER 224, GTN
Department of Energy
Washington, D.C. 20545

Dr. T. Tajima
IFS
Univ. of Texas
Austin, TX 78712

Dr. Milan Tekula
AVCO Everett Research Lab.
2385 Revere Beach Parkway
Everett, MA 02149

Dr. R. Temkin
Mass. Institute of Technology
Plasma Fusion Center
Cambridge, MA 02139

Dr. Keith Thomassen, L-637
Lawrence Livermore National Laboratory
P. O. Box 808
Livermore, CA 94550

Dr. K. Tsang
Science Applications Intl. Corp.
P.O. Box 2351
La Jolla, CA 92038

Dr. H. S. Uhm
Naval Surface Weapons Center
White Oak Lab.
Silver Spring, MD 20903

Under Secretary of Defense (R&E)
Office of the Secretary of Defense
Room 3E1006, The Pentagon
Washington, D.C. 20301

Dr. L. Vahala
Physics Dept.
College of William & Mary
Williamsburg, VA 23185

Ms. Bettie Wilcox
Lawrence Livermore National Lab.
ATTN: Tech. Info. Dept. L-3
P.O. Box 808
Livermore, CA 94550

Dr. J. Wurtele
M.I.T.
NW 16-234
Plasma Fusion Center
Cambridge, MA 02139

Dr. A. Yariv
California Institute of Tech.
Pasadena, CA 91125

END

9-87

DTIC